Characterization of Supported Catalytic Metallic Nanoparticles using Transmission Electron Microscopy

Thesis for a Degree of
Master of Science in Engineering Nanoscience

Author:
Axel Persson

Advisor:
Prof. Reine Wallenberg

June 16, 2015

LUND
UNIVERSITY

Abstract

In this project catalysts have been analyzed, in the sense of size and composition, using a Transmission Electron Microscope (TEM). This important class of substances are used to facilitate chemical reactions, in everything from specific molecular research to conversion car emissions which explains the importance of research. Nanoparticles of gold (Au) have been shown to have good catalytic performance. However, optimization in size is crucial due to the different facets present at different sizes. TEM has been used to image the catalysts, using contrast in different modes of operation to distinguish the gold from the carrier oxide which is there to prevent agglomeration of the gold. Sizes of the Au nanoparticles ranged from 5 to 16 nm without any agglomeration observed. Further, so called Molecular Imprinted Polymers, MIPs, were analyzed for their elemental content and to make sure no palladium (Pd) from the palladium containing molecules had reduced to metallic particles during polymerization. The results were promising in the sense that stable low levels of Pd without any metallic palladium were observed. TEM-modes used were different in how well they could distinguish the particles. Conventional imaging (CTEM) proved difficult since high scattering occurred from thicker oxide as well. While scanning TEM (STEM) was the preferred method due to the clearer results in its HAADF-mode (High Angle Annular Dark Field). Together with X-ray Energy Dispersive Spectroscopy (XEDS) STEM provided compelling images and elemental maps of where gold was found in the clusters. One could also pick certain points in the image to get local composition, useful for the MIP-analysis.

Svensk Sammanfattning

Detta projekt syftade till att analysera storlek och ämneskomposition av katalysatorer med hjälp av ett transmissionselektronmikroskop (TEM). Katalysatorer är ämnen som underlättar kemiska reaktioner i allt från spetsforskning inom kemi till rening av bilars avgaser, vilket gör dem mycket viktiga och motiverar forskning. Guld (Au) i form av nanopartiklar har visat sig användbara på området men deras storlek behöver anpassas för att optimera effekten. Med ett TEM har dessa partiklar avbildats och storleksbestämts genom flertalet detektorer för att kunna skilja på Au och de oxider som använts för att bära upp Au-partiklarna så de inte klumpar samman. Partiklarnas storlek bestämdes till mellan 5 och 16 nm. Ytterligare prover som analyserades var s.k. MIPs (Molecularly Imprinted Polymers, fri översättning: molekylära avtryck i polymerer). Dessa skulle sammansättningsbestämmas och undersökas huruvida molekylärt bundet palladium (Pd) reducerats till dess metalliska form under polymerisationen. Resultaten var lovande då polymeren visade stabila värden av Pd och det fanns ett prov där metallisk Pd inte återfanns. De olika detektorerna och arbetssätten i TEMet var olika användbara. För guldpartiklarna visade det sig svårt att hitta och skilja på guld och tjockare oxid då man använde konventionell TEM (CTEM). Svep-TEM (STEM) resulterade i tydligare bilder. Dessutom kunde man skapa tydliga kartor över var de olika ämnena återfanns genom analys av röntgenstrålning från provet, s.k. X-ray Energy Dispersive Spectroscopy (XEDS). Detta var också lämpligt för MIP-proverna då man kunde välja punkter i bilden för analys.

Acknowledgments

I would like to thank several people for their help making this project possible. Especially my advisor Prof. Reine Wallenberg for your overall support, giving me the opportunity and trusting me to work with the electron microscopes. Thanks also to Filip Lenrick and Gunnel Karlsson for all your help and input concerning the mentioned microscopes, and thanks to the rest of the PolyMat-group, including my fellow master thesis students, making time here very pleasant.

I would like to thank my friends and family for all the support and input. Lastly, Emma for everything above, perhaps not the electron microscopy part but the rest even more.

List of Figures

Table of Contents

Chapter 1

Introduction

"A catalyst is a substance which affects the rate of a chemical reaction without being part of its end products."[3] This is a general explanation of the class of substances called catalysts, defined by Wilhelm Ostwald around the year 1900. The phenomenon however, had been known during the majority of the previous century, described by the Swedish chemist Jöns Jacob Berzelius as early as 1835 [3]. He also coined the name *catalysis* which is derived from the Greek words for "breaking down by coming together"[4, p. 565]. Reactions using catalysts are facilitated hence increasing the likelihood of occurring.[3][5, p. 3]

Since reactions occur at the interface of the catalyst, surface area is important. Nanoparticles, which have dimensions down to a few nanometers ($10^{-9}m$), are interesting because of effects arising at that scale as well as the small volume needed to achieve high surface area. There are even metals such as gold (Au), which are not catalytically active in bulk but only at the nanoscale[6][7]. To use these in combination with other metals, such as palladium, as well as altering dimensions to optimize for the reaction at hand, have been shown useful.[8][9] Optimization of catalysts will improve many areas including chemical industry and the energy sector [10], meaning research is of benefit for all of society.

Imaging as a form of analysis has always been of importance. Images are often easily interpreted and in the case of particles would reveal size, shape and distribution. At nanoparticle scale light microscopes will not suffice. The limit of resolution is set by the wavelength and therefore energetic electrons are used, in the technique called electron microscopy.[1, p. 5] This thesis will deal with the Transmission Electron Microscope (TEM) as a tool, including its different modes and detectors, for characterization of catalytic nanoparticles of gold on carrier materials such as ceria (CeO_2) or zirconia (ZrO_2). The knowledge of size and spatial distribution, as well as the shape of the catalyst are necessary in understanding the role of the support in distributing the particles and in its properties.[11][12] The thesis also contains analysis of samples of so called Molecularly Imprinted Polymers (MIPs) and beads of tungsten-zirconia ($W - ZrO_2$).

Chapter 2

Catalysis

2.1 The Phenomenon of Catalysis

Catalysts, as described in the introduction, are substances that affects reactions without being consumed themselves. IUPAC defines them somewhat narrower and states that they not only should affect but strictly increase the rate of the reaction.[13, p. 220][14] A reaction using a catalyst is provided with alternative pathways of reaction. Meaning, the catalyst can form intermediate compounds that quickly react in additional steps (figure 2.1) in order to reach the final product, while the catalyst always is preserved. This alternative way of reaction might require less activation energy than the direct alternative, hence the increased rate of reaction in the presence of a catalyst.[4, p. 565] Many substances can act as catalysts in the right setting and the effect depends on the reactants as well as the reaction conditions such as temperature and acidity.

$$xX + yY + cC \longrightarrow zZ + cC \tag{2.1}$$

Equation 2.1 shows a general reaction including a catalyst (C), which is not consumed and can participate in the reaction again. This results in generally very low concentrations of catalyst are required.

2.1.1 Example of Reaction

The catalytic effect increases the rate significantly and it was estimated in 1993 that about 80% of the chemical products were manufactured using catalysts and for different forms of fuels the number was even higher.[5, p. v] This shows what a significant role catalysts have had for a long period of time. One of the more important reactions developed was the production of ammonia, designed by Haber in 1909. Ammonia, which is important as a fertilizer, was produced according to the process 2.2 with the help of an osmium (Os) catalyst, later improved to use the more abundant element iron (Fe). The increased capability of food production meant coping better with increasing population and resulted in Haber being awarded the Nobel Prize in 1919.[3][5, pp. 5-7][14]

$$N_2 + 3H_2 \xrightarrow{Os} 2NH_3 \tag{2.2}$$

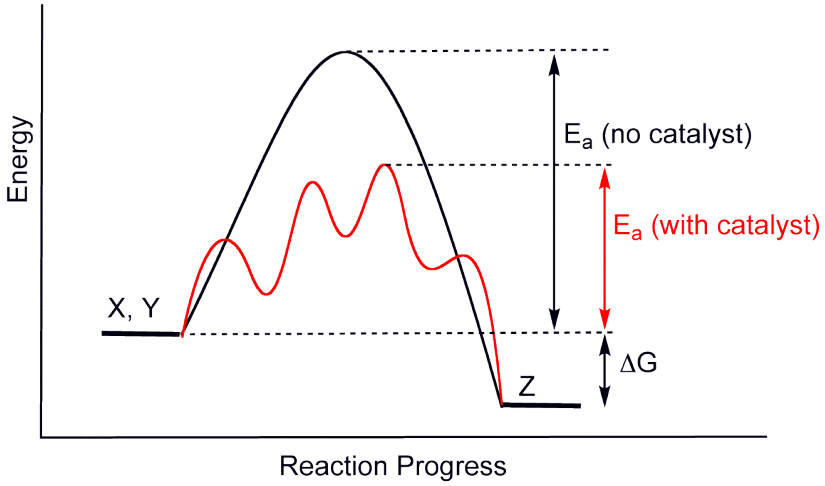

Figure 2.1: A schematic graph of the energies required for reaction. E_a is the activation energy with (red) and without (black) a catalyst. The small "bumps" of the catalyst transition are the activation between the elementary steps. Start and stop free energies are the same but the magnitude of the E_a of the partial steps are lower, hence the faster reaction.

2.1.2 Rate of Reaction

A catalyst provides elementary reaction steps for the reactants, alternative reactions to the direct, slower reaction. Since the magnitude of the activation energy is lower while using the catalyst (see figure 2.1), the rate of reaction increases. The rate will depend on the composition and structure of the catalyst, where the reactants can adsorb, react and then desorb.

$$\frac{dZ}{dt} = k[X]^n[Y]^m \tag{2.3}$$

$$k \propto e^{\frac{-E_a}{RT}} \tag{2.4}$$

The general rate equation (equation 2.3) can be used to describe the rate of formation of a product. Where n and m are constants correlating the concentrations of the reactants to the rate. k is a constant that is proportional to the Arrhenius expression (equation 2.4), i.e. involves the temperature and activation energy. Since equation 2.3 is empirical it can be modified according to the specific reaction and also include the concentration of a catalyst ($[C]^l$). Important to remember is the catalytic effect is also affected by, for example, the shape of nanoparticles as the ones used in this thesis. E_a of equation 2.4 would change when a catalyst is used, resulting in increased rate. Caution must be used with equation 2.3, as always for empirical formulas, when catalysts are added.

2.2 Nanoparticles as Catalysts

The high surface to volume ratio of nanoparticles offers increased number of sites of reaction for the reactants at the catalytic surface. The increasing fine-tuning capabilities at the nanoscale, primarily developed in the semiconductor industry, has provided knowledge useful for these catalytic nanoparticles. Controlling the size, structure and composition is key to optimizing their effect. The structure of

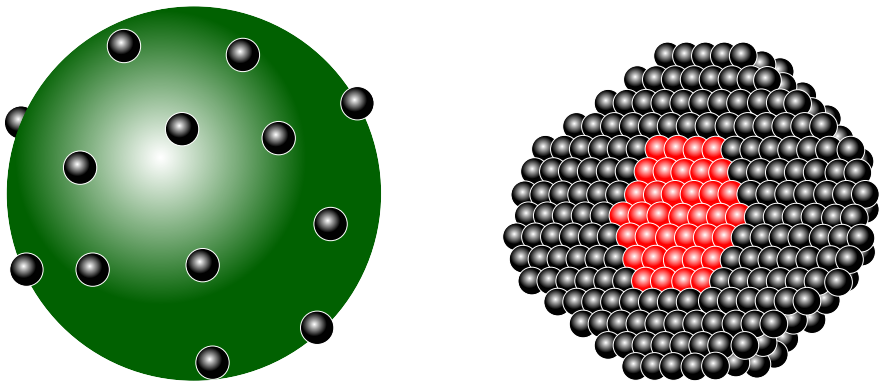

(a) Visualization of nanoparticles (black) supported on a carrier particle (green).

(b) Cut-through visualization of a core-shell structured nanoparticle. Shell-atoms (black) are surrounding the core-atoms (red).

Figure 2.2: Examples of catalytic nanoparticles and their structure. The black particles in figure 2.2a can have the structure shown in figure 2.2b.

the particle will determine which crystallographic facets will be present, facets that are distinguished by different packing planes. Different packing means different coordination of the surface atoms, leaving them chemically active which affects the catalytic performance[7]. The chemical activity of the surface atoms is due to the lack of neighbors and it also explains why smaller particles are more active. A higher ratio of the atoms in the particle are surface atoms and a large number make up steps and corners on the surface.[15, p. 2][3][7] When particles grow they tend to favor more stable surfaces, hence the lower catalytic effect. Control of which surfaces are present is vital to optimize for the specific reaction.[7]

Bimetallic catalytic particles have been reported to show better performance compared to the single metals by themselves. The synergistic effects between gold (Au) and palladium (Pd) have been investigated, especially in the form of a Au-core and a Pd-coating.[8][16][9] Optimizing the size as well as the thickness of the coating improves the performance and selectivity[8]. In figure 2.2b the structure is shown of these core-shell structures.

2.3 Supported Catalytic Nanoparticles

In the world of catalysis there are more aspects to consider than the activity. Important is also to account for mechanical stability and one way is to support the nanoparticles with larger carrier supports that either are taking part in the catalysis [17][18] or being inert [19]. These supports can disperse the nanoparticles to prevent agglomeration. For a sketch of an suggested look see figure 2.2a. Supported metallic nanoparticles are commonly used as solid catalysts for numerous applications, among them methanol production.[11]

Li et al. [17] have reported on the importance of the phase of the support in the case of active supports. In that case monoclinic ZrO_2 showed higher activity than the tetragonal form of the same support, which is believed to arise from the different coordinations of the atoms in the two phases.

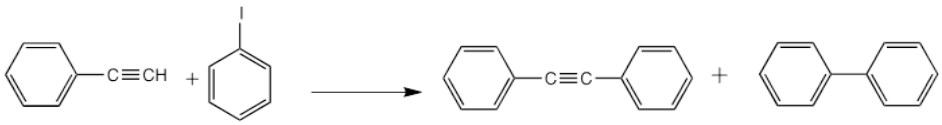

Figure 2.3: Sonogashira coupling using Au on CeO_2 or Al_2O_3 as catalyst. Products are, from left, diphenylacetylene (DPA) and biphenyl (BP).

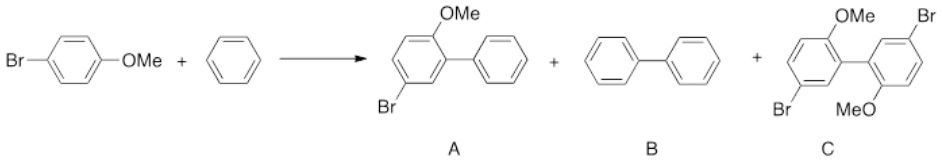

Figure 2.4: Bromoanisole coupling with benzene using Au on Al_2O_3 as catalyst.

This leads to different surface properties and therefore catalytic properties.

Some of the supported catalytic nanoparticles analyzed (Au on CeO_2 and Al_2O_3) in this thesis are used for so called Sonogashira coupling. A reaction where a terminal alkyne reacts with a aryl or vinyl halide to form a C-C bond in between.[20] This reaction is amongst others used in manufacturing pharmaceuticals[21]. The specific reaction between phenylacetylene and iodobenzene used for this catalyst is seen in figure 2.3. Au on Al_2O_3 was used for bromoanisole coupling with benzene, seen in figure 2.4.

2.4 Molecularly Imprinted Polymers

Molecularly Imprinted Polymers (MIPs) are a class of selective agents tuned to host specific molecules either for detection or catalysis. The idea is that the polymers are cured containing templates that are later removed, creating voids. Voids that are formed for a specific molecule to fit, in a specific orientation. When used as a catalyst, these voids will also host a catalytic agent facilitating a reaction for the specific molecule. The technique is mimicking natural enzymes and their highly selective catalysis.[22]

For this thesis crosslinked MIPs containing Pd (N-Heterocylic carbene palladium) as the catalyst were analyzed. The aim is to activate the C-H-bond in the molecule biphenyl through activation by the Pd-center. The activation leads to acetoxylation, where an acetoxy group is bonded to the phenyl. Activation of the C-H bonds are important because of the use of the products as raw materials in different industries[23].

Chapter 3

Transmission Electron Microscope

To be able to evaluate the size and, from that, the surface of the catalytic nanoparticles, there are several methods. One of the more common is X-ray diffraction, which through the Scherrer broadening gives average size of the particles for a larger part of the sample.[24] Secondly, there is Transmission Electron Microscopy (TEM), which renders images where the individual particles can be differentiated and analyzed.[25] This thesis is focused on using the latter because of the imaging capabilities.

The Transmission Electron Microscope is a powerful and versatile tool for imaging and analyzing samples at the sub-nanoscale. It owes its capabilities to a powerful source of electrons in combination with a series of lenses capable of adjusting the beam considering size, shape and movement. One major drawback includes the small amounts of samples analyzed at a time. The tool itself consists of a cylindrical tube kept at vacuum with a electron gun at the top. Vacuum conditions will reduce the effect of electrons accidentally scattering against air born molecules, which will reduce quality (resolution).[1, pp. 11, 127] The sample is inserted and placed in the beam to interact with the electrons, which are then picked up by a imaging system at the bottom. The JEOL 3000F TEM at The National Center for High Resolution Electron Microscopy (nCHREM) in Lund, which is used in this thesis, is shown in figure 3.1a.

3.1 Setup

The TEM-setup is a complex system of magnetic lenses responsible for guiding the electrons from the gun, through the sample and to be picked up by detectors. Figure 3.1b is a sketch of the different parts of the microscope showing the groups of lenses affecting the beam. The system can roughly be divided into three parts: the gun and illumination system (prior to the sample), the sample and lastly the imaging system (after the sample).

3.1.1 Gun and Illumination System

This top section of the microscope consists of the electron gun and the first lenses, called condenser lenses, creating the beam and transfer it onto the sample. The electron gun is a pointed tip out of which electrons are extracted and accelerated downwards. In order to be emitted, the electrons in the

(a) The microscope with controls, and computers for the detectors. (Photo courtesy Filip Lenrick)

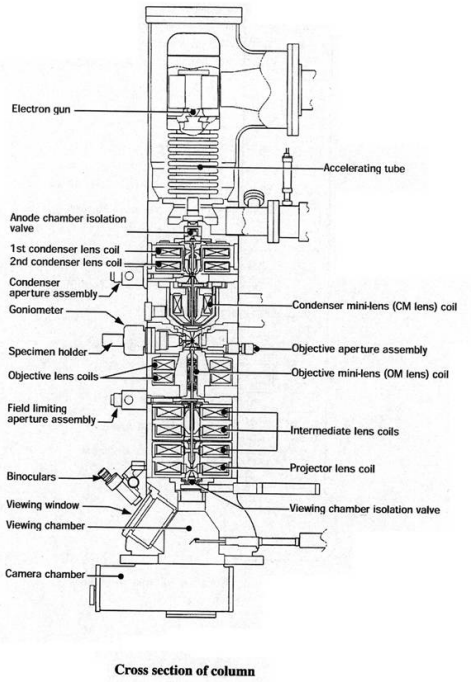

(b) Cut-through schematic of the different lens-systems and stages in the microscope. Viewed from the right in image 3.1a. (Courtesy JEOL)

Figure 3.1: The JEOL 3000F microscope at the nCHREM in Lund.

conduction band has to overcome the energy barrier from the atom, called the work function (ϕ_w). Applying an electric field ($\mathbf{E}$) together with heat will cause an increase in kinetic energy which can overcome the work function. This result in a potential energy of the electron accelerating it from the surface.

$$V(z) = \phi_w - \frac{e^2}{16\pi\epsilon_0}\frac{1}{z} - e|\mathbf{E}|z \tag{3.1}$$

Equation 3.1 describes how the energy from the electric field as well as the distance from the atomic radius (z), due to the kinetic energy, will affect the electron potential. The sign turns negative, repelling it from the surface, at sufficiently high kinetic energy. e is the elementary charge and ϵ_0 is the permittivity in vacuum. For these so called thermionic guns, high-temperature melting materials must be used to avoid melting before any emission can occur. Tungsten (W) is one example and LaB_6 is another. The latter has a lower work function resulting in less heat required.[26, pp. 77-79]

However, in the JEOL 3000F microscope another type of gun is installed, a Schottky field emission gun (Schottky-FEG), in which an increased electric field will reduce the heat needed compared to thermionic emission. This extremely fine tip is made by W with a layer of ZrO_2 and electrons are tunneled from the surface of the tip under the influence of an greater electric field. One other kind of gun is the cold field emission gun (cold-FEG), in which the temperature is lower than the

	W	LaB_6	Schottky-FEG	Cold-FEG
T /K	2700	1700	1700	300
ϕ_w /eV	4.5	2.4	3.0	4.5
δE /eV	3	1.5	0.7	0.3

Table 3.1: Comparison of the different forms of guns. W and LaB_6 are thermionic while Schottky and cold-FEG are field emission guns. δE is the energy spread emitted from the gun.[1, p. 74]

Schottky-FEG which is an older technique but more difficult to keep stable.[26, pp. 79-81]

As can be seen in table 3.1, the field emission guns requires less heat and produces electrons with less spread of energy, which is advantageous when considering chromatic aberrations (section 3.4.2). The spread can be explained from the Fermi distribution (number of states at the specific energy state, equation 3.2) of the electrons capable of overcoming the work function (ϕ_w). With elevated T, as in the case of thermionic guns, the spread will increase.[26, p. 81]

$$f(E) \propto exp(-E/kT_c) \tag{3.2}$$

The condenser lenses are responsible of collecting the electrons from the gun and forming a desired beam on the sample, called a probe. Light microscopes use glass or plastic lenses to focus. This is not the case for EM, in which circular magnetic coils forces the electrons towards the center (optical axis) in a helical trajectory according to the Lorentz force (equation 3.3). Electrons parallel to the optical axis are not affected but any lateral movement causes forces towards the center as well as perpendicular lateral forces (resulting in the helix). The tuning of this set of lenses will define the intensity, probe size and convergence angle onto the sample.[1, pp. 99-100][26, p. 90]

$$\mathbf{F} = -e(\mathbf{E} + \mathbf{v} \times \mathbf{B}) \tag{3.3}$$

$\mathbf{F}$ is the force exerted on the electron by the magnetic field, $\mathbf{E}$ is the electrical field, $\mathbf{v}$ is the velocity and $\mathbf{B}$ is the magnetic field. All these are vectors and e is the elementary charge.[1, pp. 99-100]

3.1.2 Sample

The object to be analyzed is placed in the center of the column, in the beam of electrons. Contrast in the image can result from intensity due to amount of scattering and phase distortion. Scattering increases with thickness, resulting in less intensity for thicker parts if these scattered electrons are filtered away by apertures. For high resolution imaging, phase contrast is preferred. Electrons experience changes in phase when passing through the sample and interference of these results in the image. Both scattering and phase contrast will always be produced. However, thicker samples will scatter more and reduce the resolution from the phase-contrast, limiting this mode to a thickness of a few tenths of nanometers. For the scattering-contrast the samples can be thicker.[26, p. 98] Different grinding or etching techniques are used to reduce thickness, but in the case of the nanoparticles they already have the required dimensions.

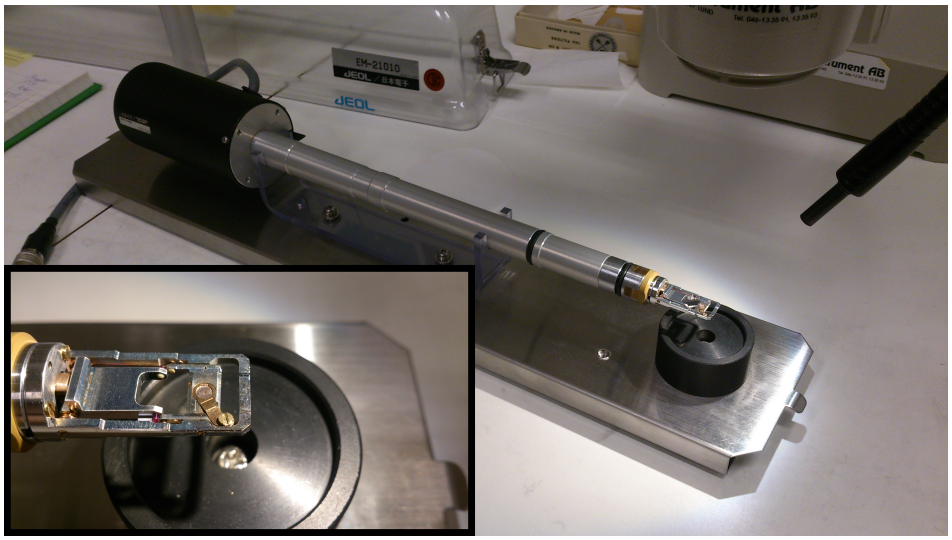

Figure 3.2: The sample holder of an TEM. In the higher magnification the tip of the holder is shown where the sample is mounted (under the arm with a screw). The tongue can be tilted and moved, making it very delicate.

The samples are placed on copper grids, with thin carbon (C) films supporting them between the grid metal (seen in figure 4.2). C is a light element and the film is amorphous, meaning it will not add any crystallinity or much absorption to the analysis. The grids are mounted in a holder (figure 3.2) and then inserted into the microscope through air-locks. The holder is usually capable of tilting the sample while inside the microscope, controlled by a goniometer. This to orient the sample so lattice fringes and other fine details become visible.[26, p. 100]

3.1.3 Imaging System

After the sample the electrons are to be projected onto the screen or CCD-camera. The sets of lenses performing this are the objective lenses, intermediate lenses and projector lenses, as shown in figure 3.3. The different magnifications are obtained by using these lenses in varying combinations of focal distances. These settings are also changed depending on the mode used (section 3.2)

The electrons scattered by the sample are focused by the objective lens, forming an image in the image plane. In the back focal plane of the objective lens a diffraction pattern forms with the electrons scattered in the same angles collected. This is the plane where the objective lens aperture is inserted, capable of filtering out the high-angle scattered electrons (more in section 3.2). The image formed by the objective lens is the most critical in terms of the quality of the resulting image, making it extra important to have a lens free of flaws. After the initial image or diffraction pattern it is magnified through the intermediate and projector lenses (figure 3.3).[26, p. 103]

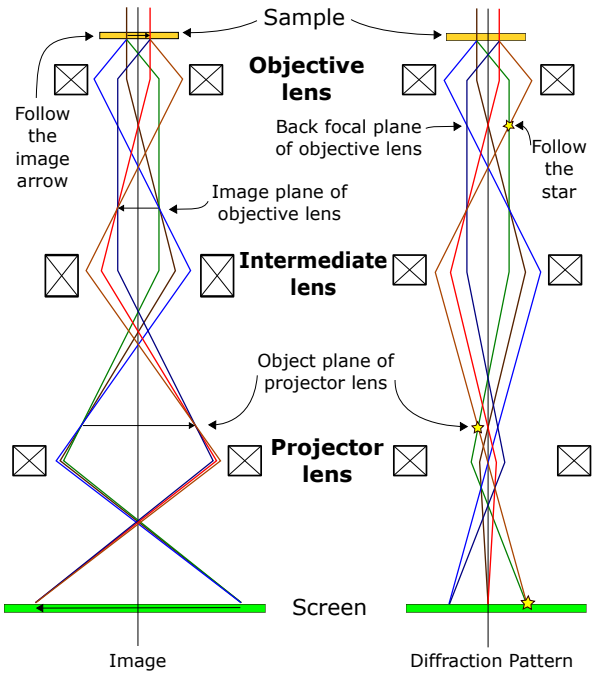

Figure 3.3: Modes of projecting the sample onto the viewing screen. The setup to the left produces a image while the right setup displays the DP. The differences in mode is decided with the strength of the intermediate lens. (Courtesy Filip Lenrick)

3.2 Modes

The versatility of the TEM is best illustrated by the differences in mode of operation. Settings in the lenses in combination with detectors used can give several aspects of the sample, confirming each other as well as giving a more complete picture. Here follows a couple of basic modes for the TEM commonly used.

3.2.1 Diffraction

Incident electrons will interact with the sample, due to charges and particle interaction. It is now important to consider the electrons as both particles but, in this mode, primarily as waves. According to Bragg's law (equation 3.4) there are certain angles (θ_B) that will produce constructive interference in crystals. These angles are relative the diffracting lattice planes, so by detecting diffraction peaks one can distinguish distances between planes (d) if the wave-length (λ) is known. n is an integer.[1, pp. 48-49]

In the back focal plane of the objective lens, the same-angle scattered electrons will collect into spots and if the rest of the imaging system is set to image this plane it will be magnified on the screen/CCD. The shape of the diffraction pattern (DP) and the relative distances between the peaks is a tell-tale of the crystal structure at hand and in what direction it is oriented. A DP in the focal plane corresponds to the Fourier transform of the image, an analysis that gives the present frequencies (k) as well as their intensities ($F(k)$) from the sample pattern ($f(x)$) (equation 3.5). The technique is often used in signal analysis over time (one dimensional), but in the case of images it is over two-dimensional space

(vector **r**), creating an two-dimensional map over the spacial frequencies (vector **u**).

$$n\lambda = 2dsin\theta_B \tag{3.4}$$

$$F(k) = \int_{-\infty}^{\infty} f(x)e^{-ikx}dx \tag{3.5}$$

This method of producing DPs is very useful and gives information about the crystal and can reveal defects or changes in the lattice. Filtering the spots, by inserting apertures in the back focal plane, can reveal which areas are responsible for a certain diffraction.

3.2.2 Conventional TEM

In the conventional TEM (CTEM) mode, the whole part of the imaged specimen is irradiated with the beam at the same time. This requires the condenser lenses to form a parallel beam of desired size hitting the site of interest. Scattering contrast in the image arises in the same way objects cast an shadow. Thicker or denser areas will scatter more, resulting in less intensity if the high angles are filtered out by use of an aperture. The setup in figure 3.3 is in CTEM.

3.2.3 Scanning TEM

When using the TEM in scanning mode, called STEM, a fine probe is focused by the condenser lenses onto the sample only getting information from a small part of the image at a time. The probe is rastered across the whole field of view to make up the whole image. Rastering is performed by deflection scan coils, situated below the condenser lenses, that slightly deviate the beam but keep it parallel to the optical axis when it hits the sample. [1, p. 158][26, p. 93] Since each spot diffracts the beam in different ways an image on the image plane is not possible. Instead one uses detectors situated differently relative the optical axis (section 3.3.2). The Bright Field-detector (BF) measures the intensity of the direct beam and the low angle scattering electrons, while the Dark Field-detector (DF) measures intensity of the more scattered electrons. The result gives us information for each point in the image, whether it scatters more or less. For the BF-detector, it gives an image with less intensity where the beam hits a less electron transparent sample. For the DF-detector the signal depends on high scattering, not as much on transparency. A high signal would mean the point of interest scatters a lot, such as a high Z (atomic number) element.[1]

The most important part to remember of the STEM-mode is that the image is not magnified by any imaging lenses. The sole parameter that decides the magnification is how far the probe moves in between each spot of detection. Since each spot will result in a intensity, this will translate into brightness of a pixel in the image. The smaller the steps between the spots, the more pixels will describe the same distance, which means the image is magnified more. The critical point is how small the probe is.[1, p. 161]

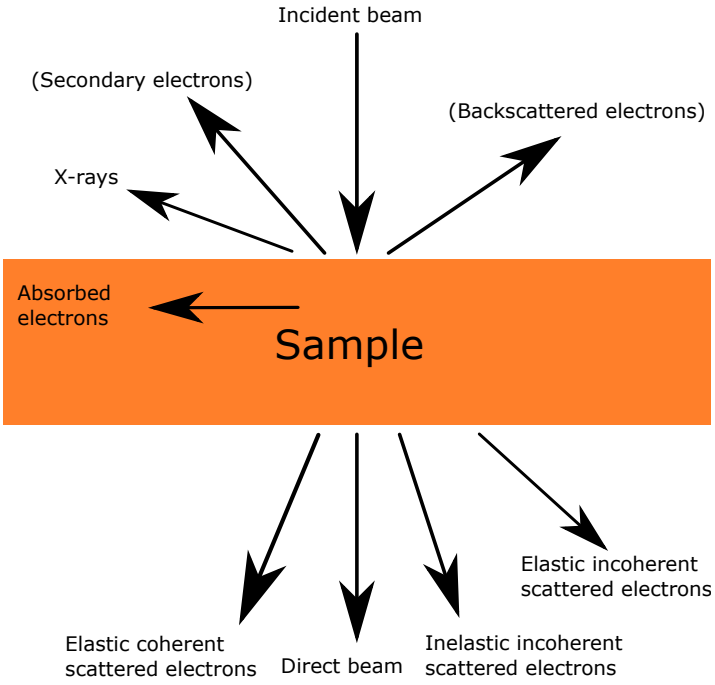

Figure 3.4: Some of the resulting signals from the incident beam when interacting with the sample. Secondary electrons (SE) and Backscattered electrons (BSE) are more used in scanning electron microscopy but they can form in the TEM. Focus of the analysis is on the forward scattered electrons in combination with the X-rays.

3.2.4 Analytical TEM

When the electrons are interacting with the sample, signals of varying kinds are produced (figure 3.4). Apart from the mentioned scattered electrons that make up DPs and images, inelastic scattering can occur that results in knocking out electrons and loss of energy for the transmitted electrons. There are analytic detectors that can use the signals created to give chemical information about the sample, hence analytical TEM (ATEM). The technique mainly used in this thesis is the x-ray energy dispersive spectroscopy (XEDS, also called EDX, EDAX or just EDS). It is a very useful technique that is used, as mentioned before, to confirm findings in images and to connect compositional differences to structures found in the images.[1, pp. 581-584]

X-rays are created when incoming electrons knock out the core-shell electrons and outer-shell electrons relaxes down in energy to fill the holes created. This relaxation results in an emission of a x-ray with a characteristic energy for that transition. When obtaining a spectrum from the sample an specific element will have a fingerprint of emitted energies.[1, pp. 53-55] Analyzing the whole spectrum and accounting for the background x-rays a quantitative composition can be established. The XEDS-signal is detected by a detector (section 3.3.3) inserted above the sample and can be performed both in STEM and CTEM-mode. The advantage of using STEM is that data for each pixel in the image is stored and can be used to create elemental maps. In the analysis of the XEDS-data, one should always consider background signals such as copper (Cu) from the instrument present the spectrum. Usually one uses a holder containing beryllium (Be) parts to minimize these signals.[1, p. 584]

3.3 Detectors

3.3.1 Screen and Camera

The viewing screen at the bottom of the TEM is coated with a fluorescent material that emits light in the middle of our visible spectrum, i.e. green, when electrons reaches it. This screen is observed by the operator through a window and is usually the way of viewing the sample while operating the microscope before acquiring images. The window is designed to block out any dangerous radiation from inside the column but still give the operator a full view.[1, p. 116]

When the desired settings are reached, a CCD-camera is used to save the image. This camera is placed under the viewing screen and only access the electrons if the fluorescent screen is lifted. Lifting the screen is not all. The projector lens must be adjusted so the image plane that was placed on the screen is moved to the camera sensor.

3.3.2 STEM Detectors

In the STEM-mode each data point (pixel) of the image is recorded by retractable detectors placed under the specimen. These detectors act just as *counters* since each point is given an intensity that will translate to the gray-scale image. The detector is a doped semiconductor that creates electron-hole-pairs when the electrons hit it. These pairs are separated and thus creates a voltage that can be detected.[1, pp. 117-118]

The circular detectors are centered relative the direct (unscattered) beam with the bright field-detector (BF) in the middle, detecting only the central beam and the only slightly scattered electrons. Annular detectors are then placed outwards from the center to form the dark field image (DF).[1, p. 122] The High-Angle-Annular-DF-detector (HAADF) is the furthest from the center and some microscopes, including the JEOL 3000F only have the BF and HAADF detectors. The HAADF detector is placed at a sufficient angle from the center to minimize the contribution from diffraction, giving it the best possible Z-contrast due to the high scattering from heavier elements.

3.3.3 XEDS Detector

The XEDS-detector is a semiconductor electrode, commonly silicon (Si) which is lightly doped to form a p-i-n junction. When the x-ray reaches the detector electron-hole-pairs are formed which are detected as pulses with the help of a bias over the detector. The amount of electron-hole pairs are proportional to the energy of the x-ray making the energies differentiable. The amount of x-rays for each energy *window* is added up and make up the spectrum for that spot on the sample.

To make the detector work properly it must be cooled and protected. Cooling with liquid N_2 helps avoiding noise in the detector and amplifier as well as hinders diffusion of dopant atoms. Windows helps protect the detector but still letting the x-rays through. They are made from beryllium (Be) or special thin polymers.[1, p. 585-588]

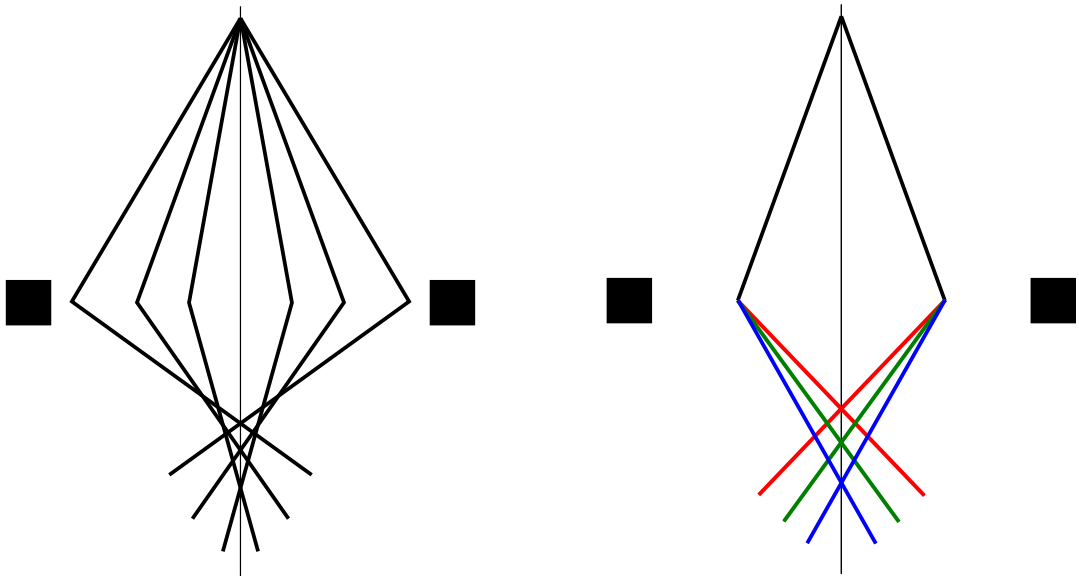

(a) Spherical aberrations **(b)** Chromatic aberrations

Figure 3.5: Schematics of the two forms of aberrations in the lenses. The electrons are originating from a common point (sample or gun) but are not focused properly, leading to a diffuse image.

3.4 Important Concepts in TEM

3.4.1 Spherical Aberrations

Spherical aberration is the phenomenon in which rays entering a lens do not converge perfectly into a point after the lens. This effect increases for rays at an larger angle from the optical axis and will form a central maximum along with decreasing intensity from the center (figure 3.5a), which is not ideal for high resolution. There are advanced sets of magnetic correctors for dealing with the problem, but many microscopes including the JEOL 3000F does not have one, which limits the resolution.[1, pp. 103-104]

3.4.2 Chromatic Aberrations

This is the second form of aberration which is not as important as spherical aberration. However, if the spherical aberration is corrected this can limit the resolution. The name indicates the analogy of colors, more specifically wavelength. Slight energy differences of the electrons, due to the gun or interaction with the specimen, will mean different wavelengths and also different interactions with the lenses (figure 3.5b). Lower energies or longer wavelength will bend more in the lens, but because of the narrow energy spread, this is not a huge problem, only limiting in the best microscopes.[1, pp. 105-106]

3.4.3 Astigmatism

Further, there can be imperfections in the magnetic lenses due to shape or microstructure anomalies in the iron core of the magnet. The effect on the electron is inhomogeneity while spiraling down. Luckily

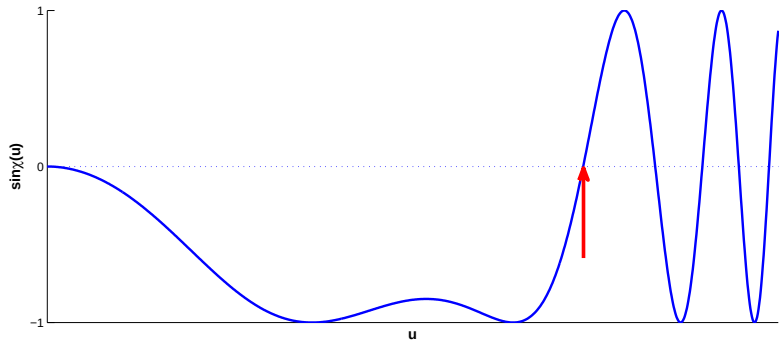

Figure 3.6: The graph illustrates the look of the CTF ($sin\chi(\mathbf{u})$) as a function of frequency $\mathbf{u}$. The first crossover, indicated by the red arrow sets the point resolution limit.

this imperfection can be corrected by using extra magnets, called stigmators, that introduces an extra magnetic field to correct the inhomogeneity. There are stigmators for both the condenser and objective lenses.[1, p. 106]

3.4.4 Contrast Transfer Function

The contrast transfer function, or CTF, describes how different spatial frequencies from the image are transfered onto the image in phase contrast imaging. This complex analysis involves the Fourier transform of the sample (as shortly described in section 3.2.1), which results in the different spatial frequencies ($\mathbf{u}$) present. In short it describes how distorted the spatial frequencies becomes from the sample ($f(x, y)$) to the image ($g(x, y)$) (equation 3.6).

$$G(\mathbf{u}) = H(\mathbf{u})F(\mathbf{u}) \tag{3.6}$$

H($\mathbf{u}$) depends on $sin\chi(\mathbf{u})$ (equation 3.7), the distortion equation, which in return depends on the settings and properties of the setup such as defocus (Δf), electron wavelength (λ) and spherical aberration (C_S).

$$\chi(\mathbf{u}) = \pi\Delta f\lambda\mathbf{u}^2 + 0.5\pi C_S\lambda^3\mathbf{u}^4 \tag{3.7}$$

Apertures in the back-focal plane can be used to cancel out the higher frequencies that have been distorted differently, thereby creating a more even distortion which makes the image easier to interpret. The highest transmitted frequency that have not been inversely distorted sets the limit of resolution. Optimizing settings for $\chi(\mathbf{u})$ will improve resolution by moving the first *crossover* in the equation, where distortion inverts, (marked with red arrow in figure 3.6) to higher frequencies.

3.5 Scanning Electron Microscope

The Scanning Electron Microscope (SEM) is another form of electron microscope, similar to the TEM in many ways but operating at lower accelerating voltages and detecting electrons on the same side of the sample as the beam enters (top side of the sample in figure 3.4). Samples can be bulk and no restrictions on thickness, other than what fits in the vacuum chamber, exists since the electrons are not supposed to pass through. A thin conducting coating can be added if the samples are not conducting the electrons away from the beam.[26, pp. 12-13]

The beam is rastered across the sample in the same fashion as in a STEM. Detectors that are placed over the sample counts the electrons for each pixel before moving along. Differences in intensities depends on the detector used. Secondary electrons (SE) are important for revealing surface topography. The signal is created when beam-electrons knock out electrons in the sample and they escape the surface. These electrons have low energy and must therefore come from a volume close to the surface to be able to escape. Edges in the sample will appear brighter since a larger portion of the created SEs can escape. Backscattered electrons (BSE) are the incoming beam-electrons that have scattered and eventually are turned back and escapes the surface. These have higher energy than the SEs and the signal will depend on how heavy the sample scatters back the incoming electrons. Heavier elements (high Z) will scatter more and therefore appear brighter in the image.

Chapter 4

Experimental

4.1 Synthesis of Particles

The catalysts analyzed were produced by researchers at the Kemicentrum, Lund University. The supported Au-particles on ceria, zirconia and alumina were produced by Sheetal Sisodiya through incipient wetness impregnation (Imp), sol-immobilization (SOL) and deposition-precipitation (DP). These techniques involves mixing Au-salts and the carrier, performing different steps related to the technique and then slowly drying them to a solid. The loading of Au in all catalysts were 3 wt%. For Imp and DP the dissolved Au-salt was mixed with the carrier oxides, for DP pH adjusted to 7 and washed several times, and lastly dried. For the SOL polyvinyl alcohol is mixed with the aquated Au-salt, reducing agent $NaBH_4$, acid H_2SO_4 and carrier oxide. The mix then is dried to form the nanoparticles.

The MIPs were produced by Maitham Majeed through free radical polymerization of a monomer containing the Pd-complex (N-Heterocyclic carbene palladium), and divinylbenzene (DVB) as a crosslinker in a 1:4 ratio (figure 4.1). The Phenyl Pyridine (two outer aromatic rings) is later removed to form the cavity for the biphenyl. Three samples were analyzed: C1 which is the top product in figure 4.1 (green), B3 which is the bottom (pink) and lastly A3 which is the C1 with the aromatic rings removed. Lastly, commercial tungsten-zirconia particles (10wt% WO_3) were analyzed. Three samples; fresh (unaltered), sintered (heat treated) and beads after being used as catalyst by Hulteberg et al. [27].

4.2 Microscopy

Focus has been on finding and characterizing the catalytic metals within the clusters of the carrier particles. The data presented shows the summarized general characteristics for the catalyst. The supported Au-particles were delivered as a powder which were dispersed into ethanol and mixed to spread the particles as much as possible. The TEM-grid was dipped into the dispersion to catch the particles on its carbon film. Figure 4.2 shows the openings in the TEM-grid, which is covered with a holey carbon film. After the grid was dipped into the dispersion some particles have sticked onto it (especially seen in figure 4.2b).

Using CTEM-mode the grid was examined, searching for high contrast particles, indicating denser

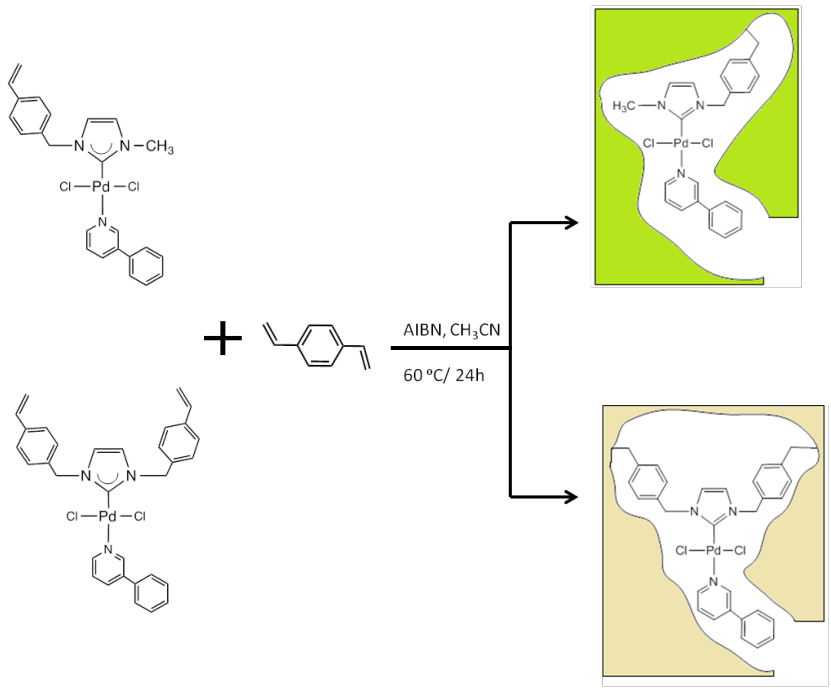

Figure 4.1: Polymerization of the monomers containing th Pd-complexes together with DVB forming the cavities when the two outer aromatic rings are removed. (Courtesy Maitham Majeed)

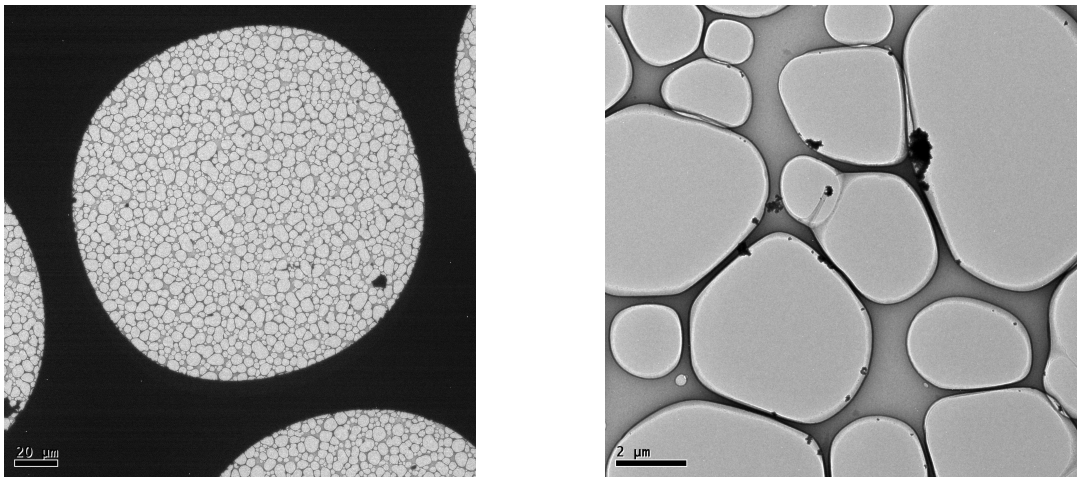

(a) A opening in the Cu grid with the holey C film visible. Scale bar is 20 μm. **(b)** Closeup on the C film with some particles visible on its surface. Scale bar is 2 μm.

Figure 4.2: Low-mag TEM images of the Cu grid and the C film.

areas as well as Z-contrast. For instance Au should scatter more, since it is more tightly packed than any of the oxides. Atomic-plane fringes were especially interesting since they can correspond to the planes and their actual distances, and if measured, they can be labeled and matched to the structure. FFT-analysis (Fast Fourier Transform) was performed of areas of interest as well as the whole images. According to equation 3.4 certain planar distances corresponds to certain angles of diffraction. The analogous Fourier transform reveals the planar distances from an image and can indicate for instance Au if higher intensities are found at specific distances from the center of the FFT. The FFT can also be filtered and inverted in order to map the areas responsible for that frequency. This is used for differentiating parts of structures from each other [28] and could be used in the case of supported nanoparticles to distinguish the Au-particles from the supporting oxide. For Au the reciprocal distances for the 111 and 200 planes are 4.24 nm^{-1} and 4.90 nm^{-1}.

The XEDS-detector was used in CTEM mode by focusing the probe on clusters and trying to find the catalytic elements. For greater spatial accuracy and elemental maps, STEM-mode was used. HAADF-analysis was used to reveal brighter spots within the clusters, that could correspond to the heavier metal catalysts.[9] Using it in combination with XEDS to map out an area gives a more complete picture. The elements analyzed, and hence spectrum compared to, in this thesis are presented in table 4.1.

	$K_{\alpha1}$	$K_{\alpha2}$	$K_{\beta1}$	$L_{\alpha1}$	$L_{\alpha2}$	$L_{\beta1}$	$L_{\beta2}$	$L_{\gamma1}$	$M_{\alpha1}$
Zr	15.775	15.691	17.668	2.0423	2.0399	2.1244	2.2194	2.3027	
Pd	21.177	21.020	23.819	2.8386	2.8333	2.9902	3.1718	3.3287	
Ce	34.720	34.279	39.257	4.8402	4.8230	5.2622	5.6134	6.052	0.883
W	59.318	57.982	67.244	8.3976	8.3352	9.6724	9.9615	11.286	1.7754
Au	68.804	66.990	77.984	9.7133	9.6280	11.442	11.584	13.381	2.1229

Table 4.1: Characteristic x-rays from the elements analyzed. Values given in keV for the different transitions present.[2]

For the samples of molecular imprinted polymers, the interesting parts were not the crystal structure but instead the elemental content. XEDS was used to quantify and map the particles that were embedded in EPON (polymer for fixing the particles before slicing). Preparation, including fixing, slicing and mounting on TEM-grids was done by other researchers.

The last sample, containing W and zirconia, was analyzed in the SEM instead of the TEM. Particle size as well as composition were evaluated using SE and XEDS-detectors. The delivered beads were mounted on SEM-stubs and some of the split open to show the inside and "particle dust" (figure 4.3). Three samples were analyzed; one freshly made, one sintered at 1000°C, and one used as catalyst for glycerol dehydration by Hulteberg et al.[27] First analysis was done with a coating layer of C. When incoming electrons hit the samples they must be conducted away from the site of impact, otherwise charging will affect the new electrons hitting the sample. The solution is to cover the surface with a thin conducting layer. C is used to give good XEDS-signals instead of a metallic coating layer due to its lower absorption of x-rays.[29]

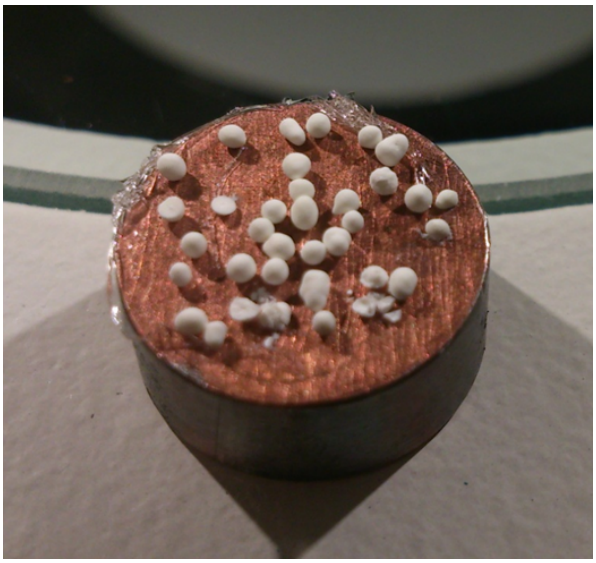

Figure 4.3: Beads of the $W - ZrO_2$ mounted on SEM-stub. Some of the beads are split in order to expose the inside.

Chapter 5

Results and Discussion

5.1 Gold on Ceria, Incipient Wetness Impregnation

The acquired images from the Au on ceria (Imp) sample are presented in figures 5.1 and 5.2. The FFT-analysis was performed on the CTEM images, such as in figures 5.3 and 5.4. XEDS-data of 16 sites (particles suspected to be Au) were acquired and presented as an example spectrum and minimum, maximum and average values in figure 5.5

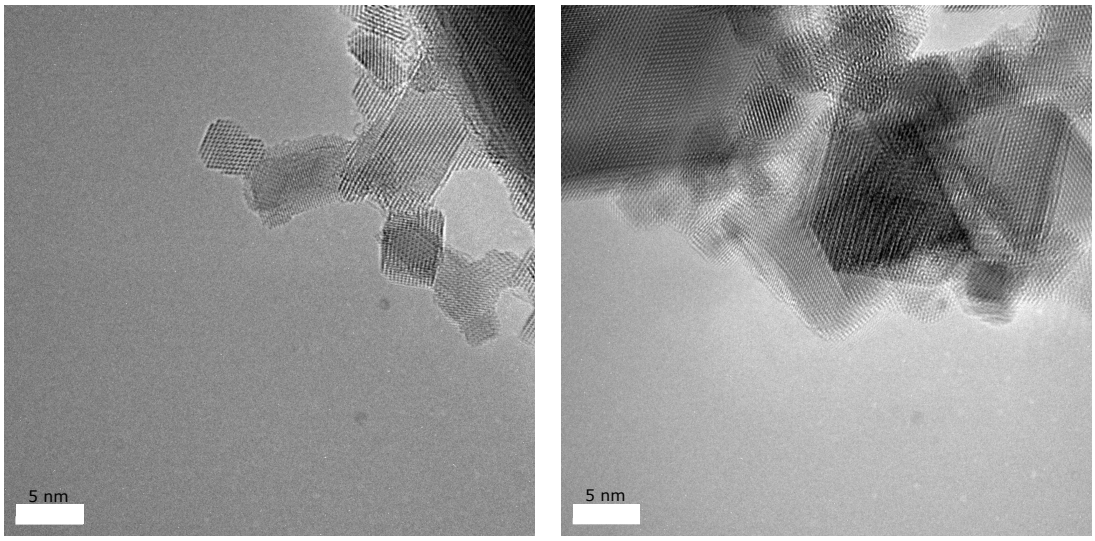

(a) A couple of protruding particles. **(b)** Cluster of smaller particles.

Figure 5.1: CTEM images of the Au on ceria sample.

XEDS-data indicates the presence of Au in the sample and that the amount is small at the sites analyzed, perhaps due to the Au being embedded. From figures 5.1 and 5.2 there are no clear evidence of the Au particles but brighter areas in the STEM-images could suggest heavier elements but nothing of certainty. The reciprocal distance of $3.25nm^{-1}$ in figure 5.3 indicates ceria and its 111 planes. Searching and filtering the FFT for the 111 and 200 planar distances of Au, such as in figure 5.4, results in finding particles with a size range from 5 to 8nm. This size is also corresponding to the brighter particles in the STEM-images, which are 7 to 8nm. The distribution of Au looks random and not agglomerated.

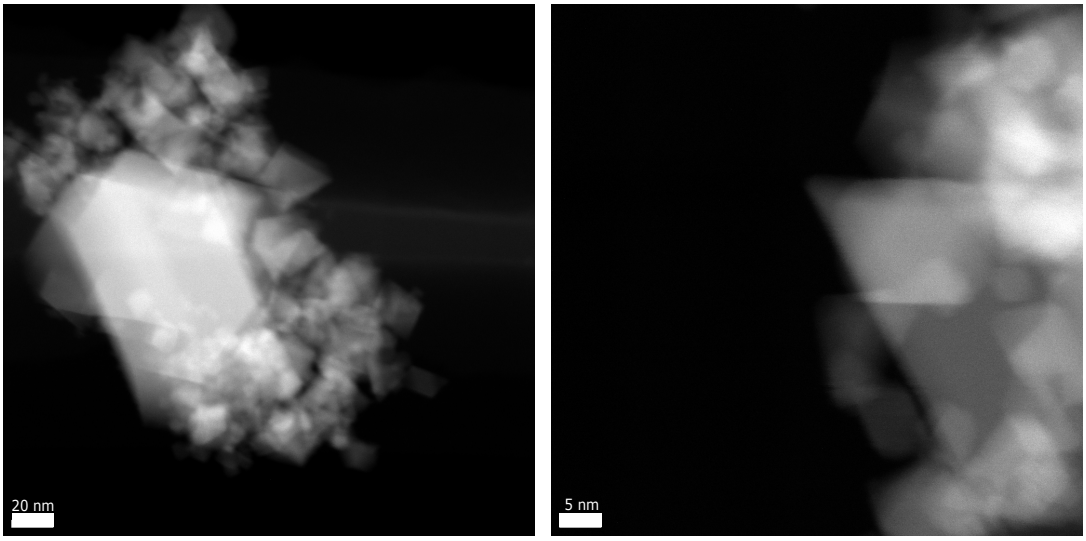

(a) Cluster of particles on the visible carbon film. **(b)** Tip of sample in cluster of particles.

Figure 5.2: STEM images of the Au on ceria (Imp) sample.

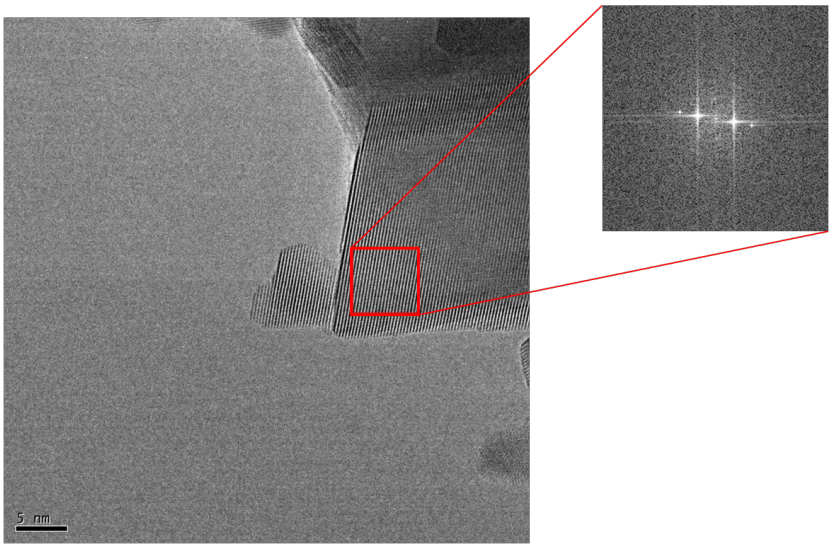

Figure 5.3: Reduced FFT of a selected area. Peaks in the pattern are at 3.25nm^{-1} reciprocal distance.

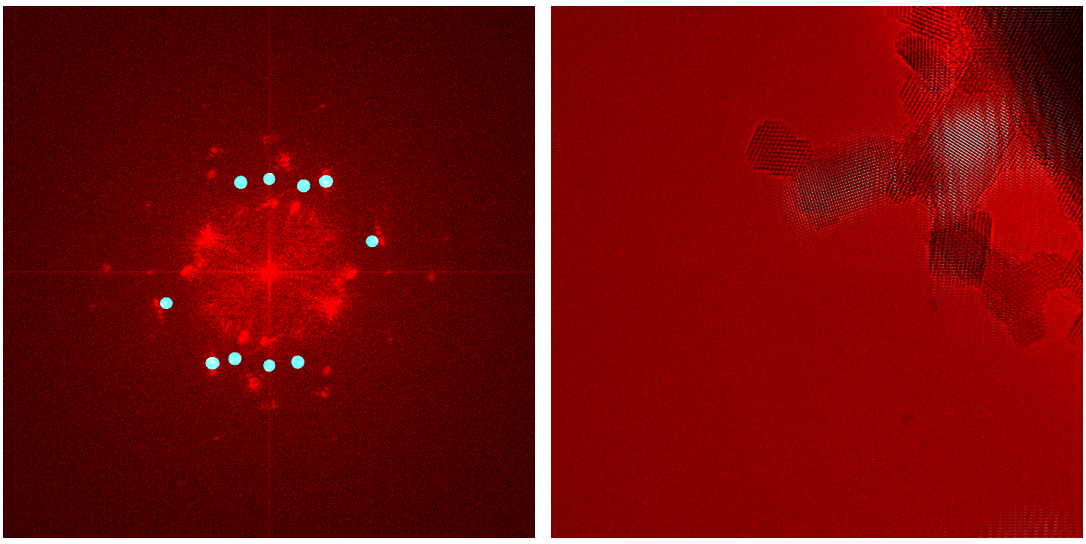

(a) FFT of figure 5.1a in red with mask selecting high intensities which corresponds to the 111 or 200 spacings of Au.

(b) Inverted FFT of the masked area of figure 5.4a (blue) over the original figure (red).

Figure 5.4: FFT-filtered image of figure 5.1a.

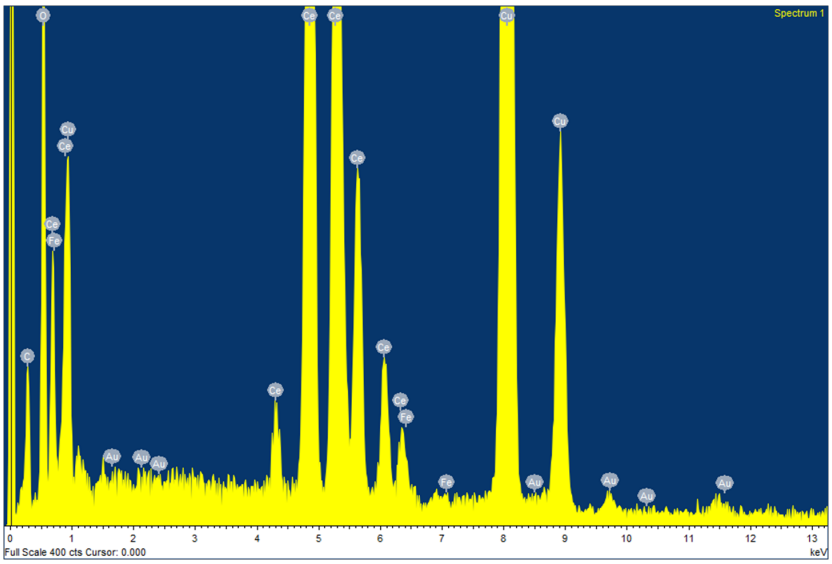

	Ce	O	Au
Max	62.61	66.27	0.96
Min	33.28	36.67	0.43
Avg	45.80	53.49	0.71

Figure 5.5: One example of the XEDS-spectras from Au on ceria (Imp) sample. The table shows the quantification-data for 16 measurements in atomic%.

5.2 Gold on Ceria, Sol-Immobilization

For the second method for Au on ceria, SOL, CTEM images were acquired (figure 5.6) which were analyzed by FFT in figures 5.7, 5.8 and 5.9. XEDS-data for 13 measurements (particles suspected to be Au) is presented in table 5.1.

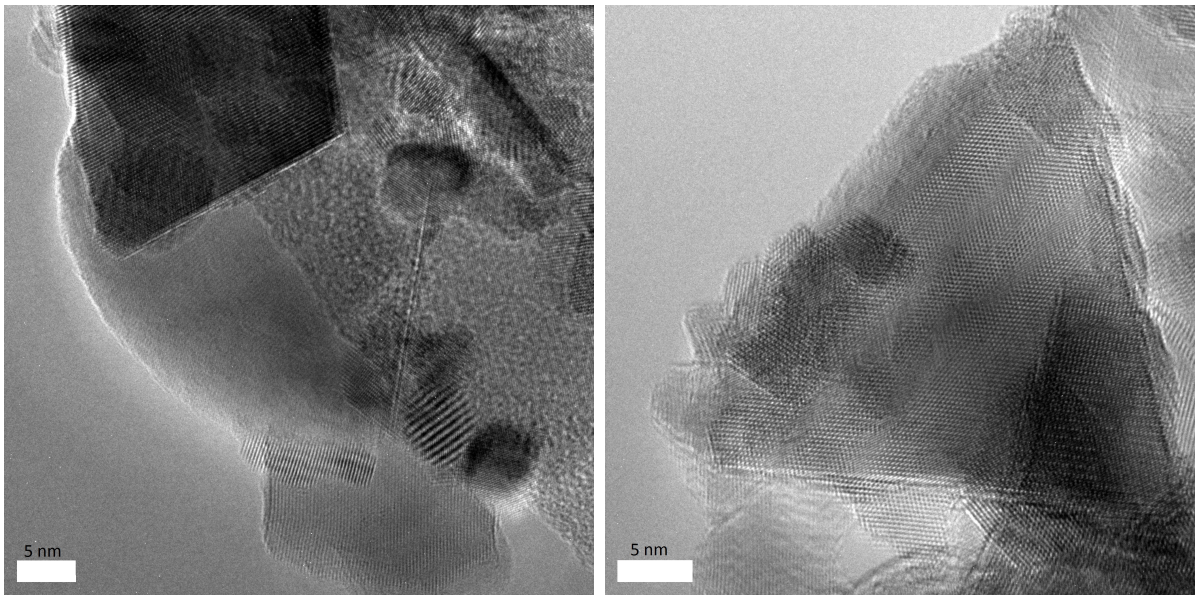

(a) Particles with "suspect" smaller particles on top. **(b)** Some more "suspect" particles.

Figure 5.6: CTEM images of Au on ceria (SOL).

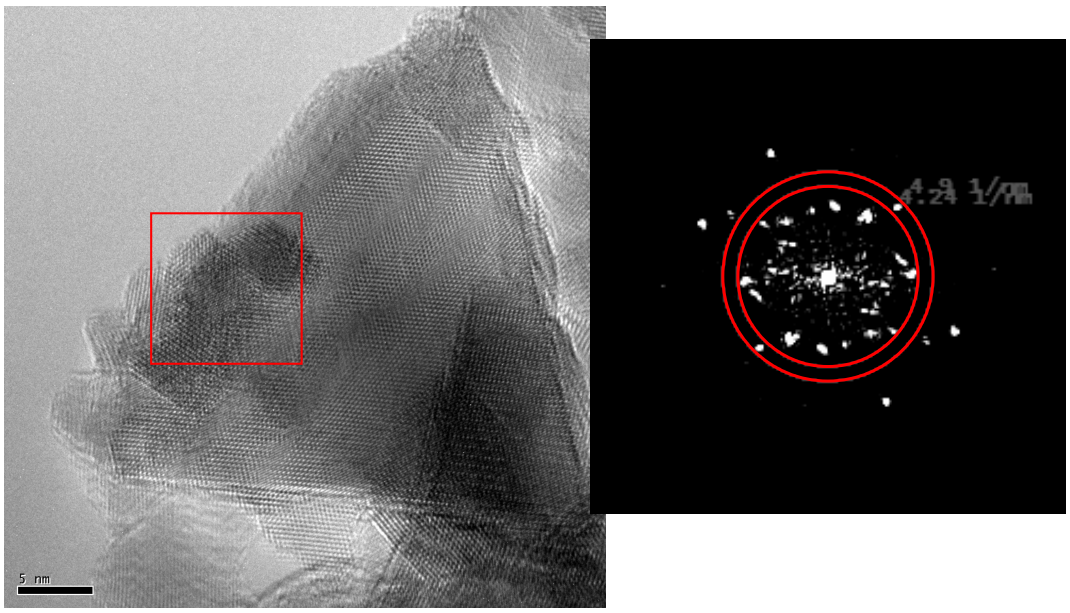

Figure 5.7: FFT analysis of image in figure 5.6b. Circles corresponds to gold 111 and 200 planar spacings.

From the images the structure seems similar to the Imp-sample, with particles of varying size. However, from the XEDS-data the Au-signal is significantly higher at some of the measurements, suggesting more

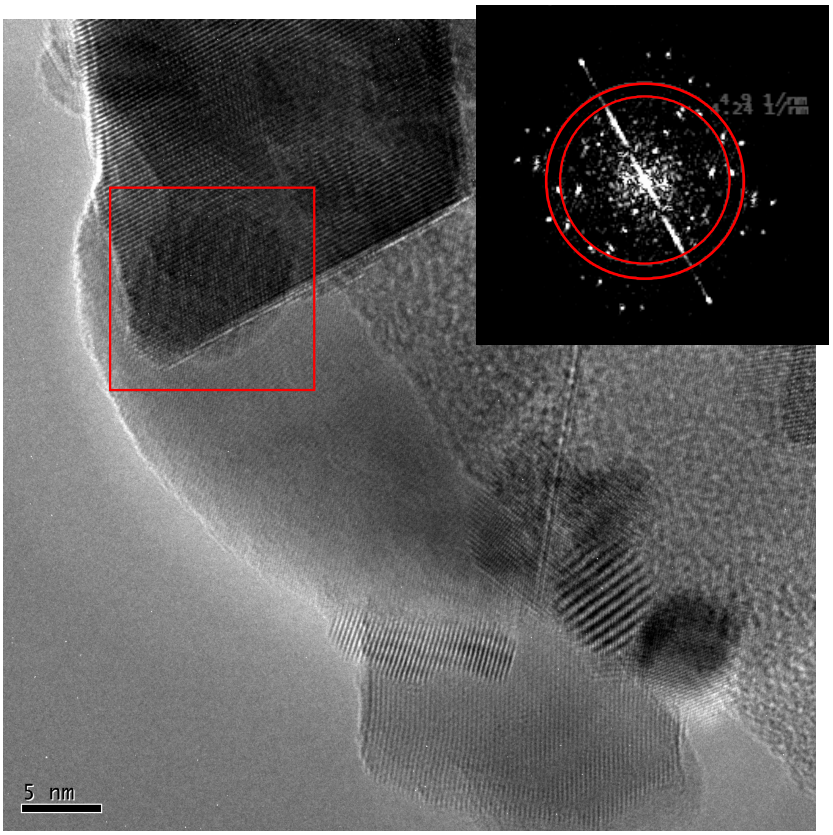

Figure 5.8: FFT analysis of a 11nm particle in Au on ceria (SOL) sample. Circles are corresponding to 111 and 200 planar spacings of Au.

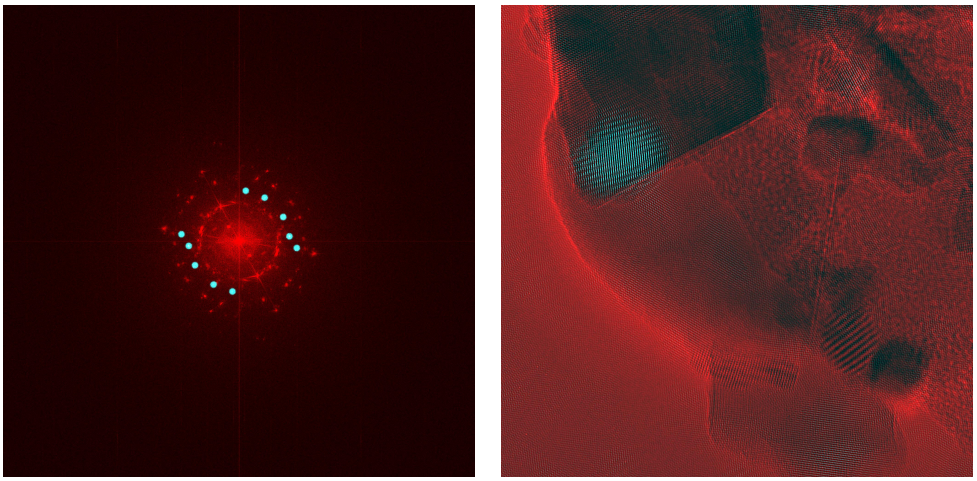

(a) FFT of figure 5.6a in red with mask selecting high intensities which corresponds to the 111 or 200 spacings of Au.

(b) Inverted FFT of the masked area of figure 5.9a (blue) over the original figure (red).

Figure 5.9: FFT-filtered image of figure 5.6a.

Au since the intensity relates to the amount. More Au results in the electron beam not hitting as much oxide, giving less portion of the signal from the oxide. Some particles supposed to be Au however do not show any Au-signal, suggesting not all dark particles are Au. When the CTEM-images are analyzed

	Ce	O	Au
Max	89.23	95.54	11.73
Min	4.46	9.33	-0.06
Avg	33.07	65.42	1.51

Table 5.1: XEDS data from the gold on ceria (SOL) sample. All data given in atomic%.

by FFT in figure 5.8 and 5.9 one particle is found with signs of the planar distances associated with Au, but not in figure 5.7. Figure 5.9 indicates a particle with fringes indicating Au. The size of that particle is 11nm and other found particles range from 9 to 12nm.

5.3 Gold on Zirconia, Deposition-Precipitation

The sample was analyzed with CTEM (figure 5.10) and STEM images (figure 5.13). Au-particles are searched for through FFT-analysis (figure 5.11 and 5.12) and XEDS-measurements for 16 particles suspected to be Au (table 5.2).

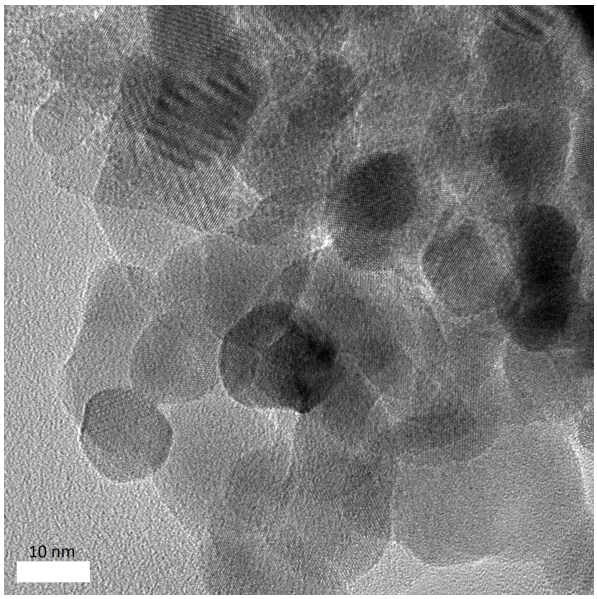

(a) Cluster of particles.

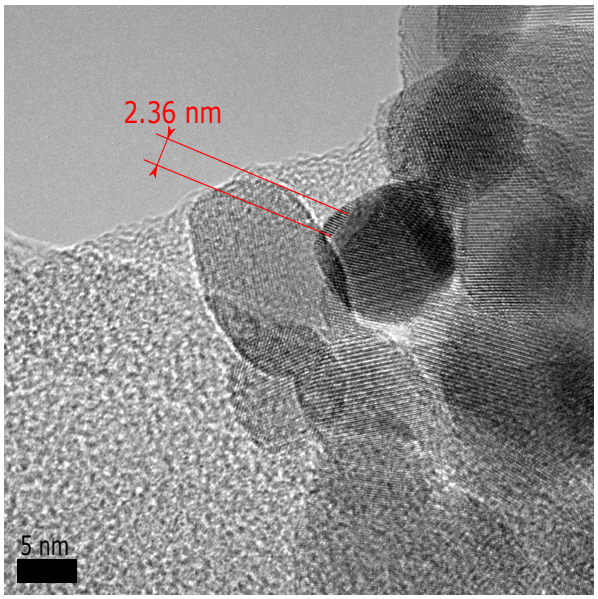

(b) Some particles on the amorphous carbon film. 10 fringes of the exposed particle are marked and measured to 2.36nm. The spacing of 2.36Å correlates to Au 111.

Figure 5.10: CTEM image of Au on zirconia.

	Zr	O	Au
Max	59.9	92.4	24.1
Min	0.65	39.66	0.13
Avg	34.70	60.30	5.00

Table 5.2: XEDS data from the gold on zirconia (DP) sample. All data given in atomic%.

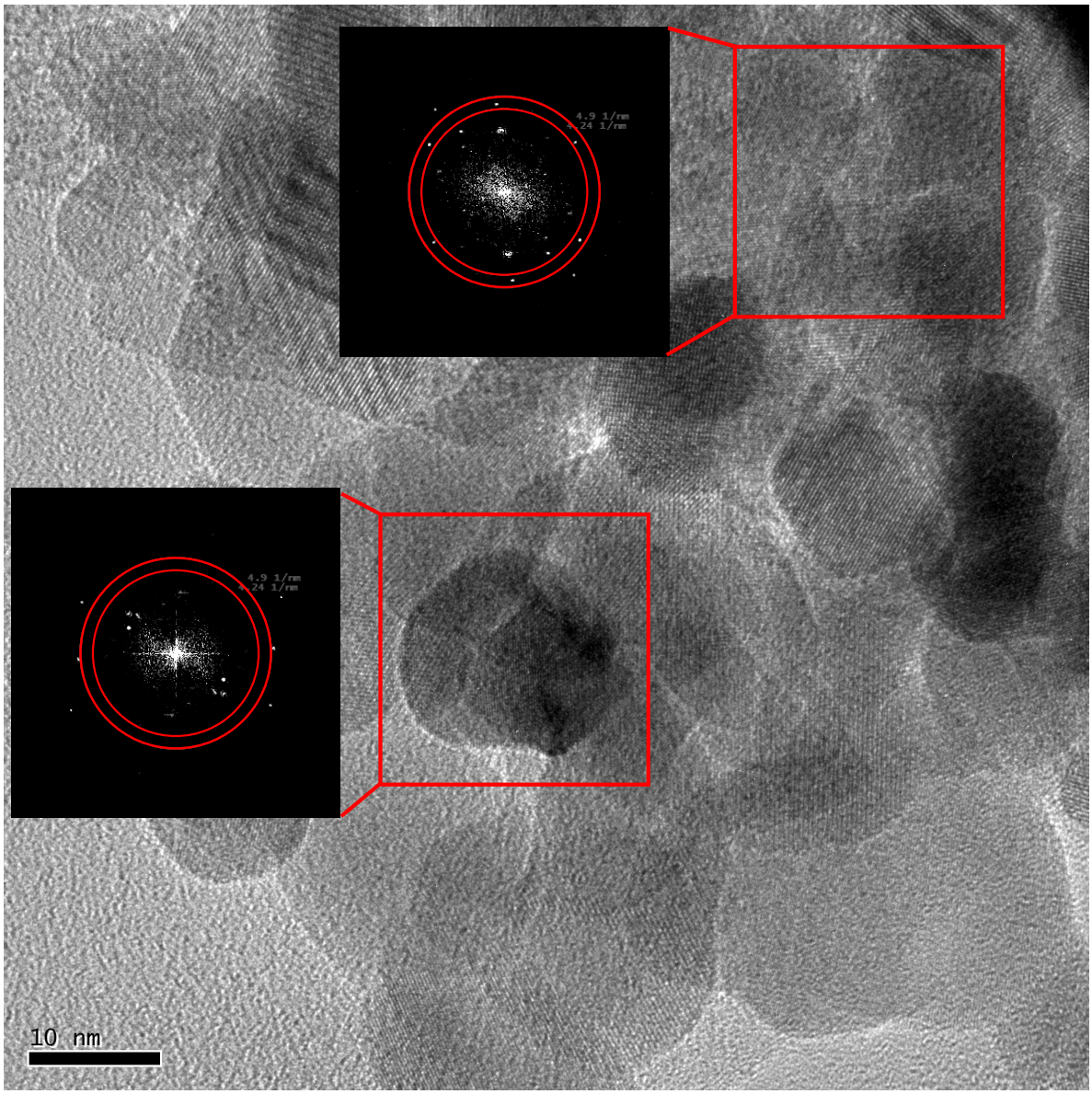

Figure 5.11: FFT-analysis of selected areas from a TEM-image of Au on ZrO_2. The two black images are the FFTs of the marked areas with circles pertaining to reciprocal spacings for 111 and 200 planes of Au. For the top FFT, there seems to be no distinct peak at the rings. Peaks that are found in the lower FFT.

A couple of particles were found which were established to be Au through FFT and measurements in the image. Their sizes were between 8 to 16nm found both in CTEM and STEM images. Correlation between XEDS-maps and STEM-HAADF were found in figure 5.13 in which brighter particles equals Au. One particle was found in figure 5.10b that had accessible fringes, free from any overlap. The distance of 2.36Å correlates to the 111 planes of Au.

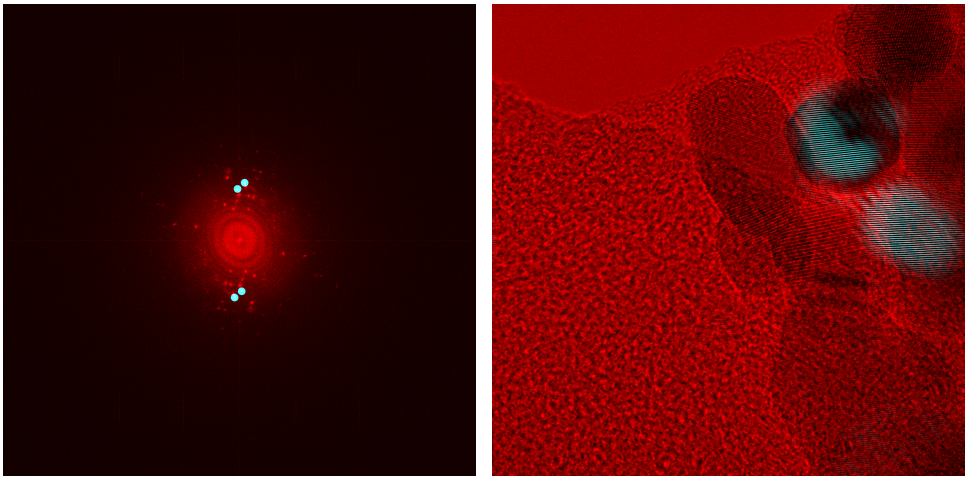

(a) FFT of figure 5.10b in red with mask selecting high intensities which corresponds to the 111 or 200 spacings of Au.

(b) Inverted FFT of the masked area of figure 5.12a (blue) over the original figure (red).

Figure 5.12: FFT-filtered image of Au on zirconia.

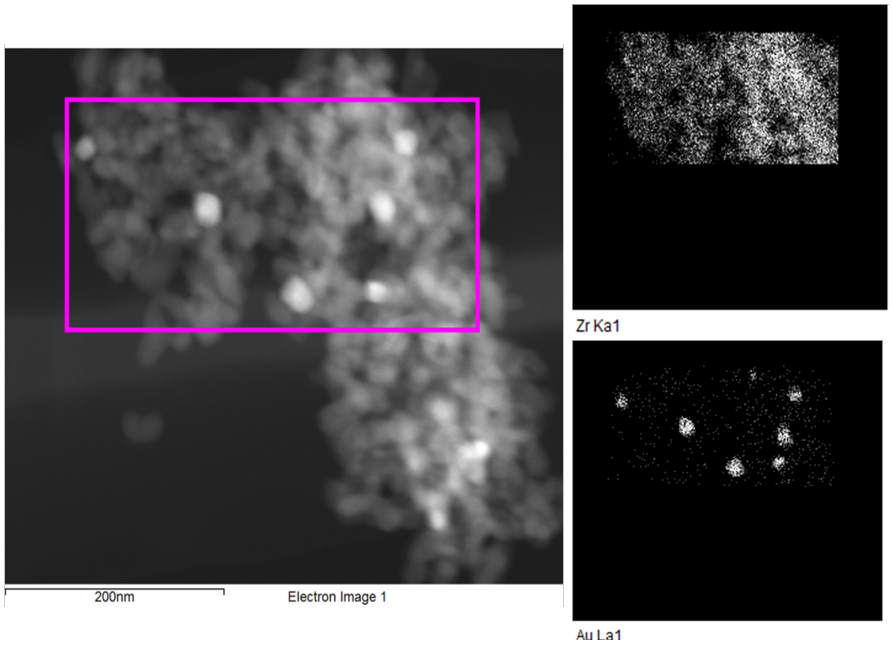

Figure 5.13: HAADF-STEM images with XEDS-map of one of the clusters in Au on zirconia sample. Zr and Au are the elements mapped.

5.4 Gold on Alumina, Incipient Wetness Impregnation

For this sample, focus was set on large quantities of CTEM images (from the researchers producing the samples). Figure 5.14 shows examples of these where figure 5.14b is FFT-filtered for the Au planar spacings 111 and 200 into figure 5.15.

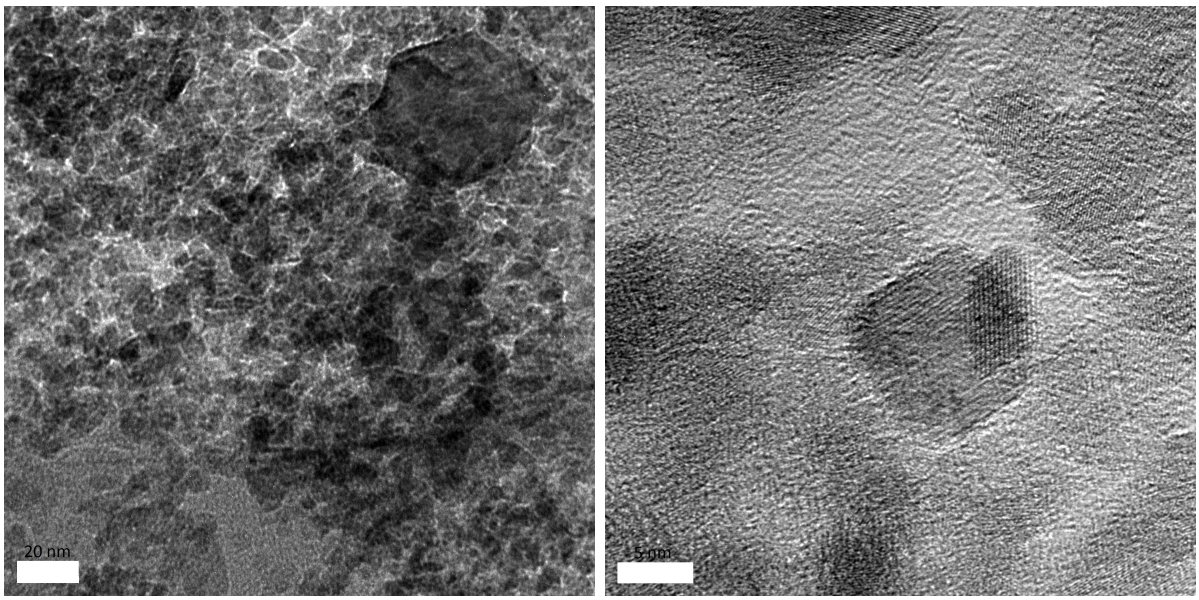

(a) Cluster of small particles used for trying to distinguish Au from the alumina.

(b) Higher magnification of a particle, 12nm in size.

Figure 5.14: CTEM images of Au on alumina.

As seen in the FFT-filtered image (figure 5.15), the particle does not correlate to Au but instead there are other areas corresponding to the specified planar spacings. These areas were approximated to particles of 7 to 10nm in size. The lack of fringes correlating to Au from the particle in figure 5.14b does not completely exclude it from being Au, it could just be misaligned in a fashion not revealing any fringes.

The results from all the Au on oxide samples are shown in table 5.3. Also included are the catalytic results from using the catalysts for the designated reaction. These tests were given by the researchers producing the catalyst.

Au on:	Size /nm	Catalytic measurements
CeO_2 (Imp)	5-8	DPA: 66%
CeO_2 (SOL)	9-12	
ZrO_2 (DP)	8-16	A: 59%, B: 39%, C: 2%
Al_2O_3 (Imp)	7-10	DPA: 61%

Table 5.3: Summarization of the size of the particles found in the different samples of supported Au-particles. Including are the catalytic performance for each of the samples tested by other researchers.

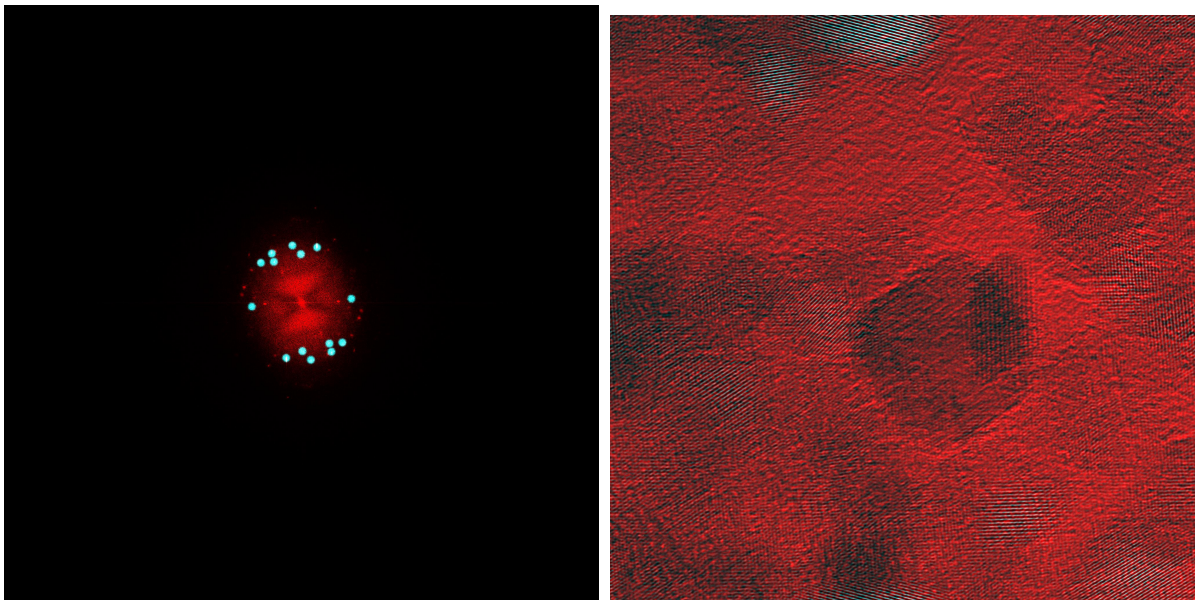

(a) FFT of figure 5.14b in red with mask (blue) selecting high intensities which corresponds to the 111 or 200 spacings of Au.

(b) Inverted FFT of the masked area of figure 5.15a (blue) over the original figure (red).

Figure 5.15: FFT-filtered images of Au on alumina.

5.5 Palladium Containing Molecularly Imprinted Polymers

An XEDS-analysis for the MIP-particles is shown in figure 5.16 (sample A3), taken with BF-STEM. The darker areas are the particles while the brighter are the fixating polymer. CTEM is also used for a smaller darker particle found in the MIP (figure 5.17b).

The quantification from the XEDS shows a stable value of the Pd and Cl content in the MIP-particles, which also was consistent for measurements of the other samples. Outside the MIP the Pd and Cl content was almost 0%, correlating to the polymer EPON that does not contain those elements. In figure 5.17b a faint periodicity was found and analyzed using FFT. The pattern revealed a reciprocal distance of 4.45nm^{-1} which correlates to metallic Pd and its 111 planes with 2.25Å spacing. This is also confirmed by the higher Pd signal obtained by the XEDS-detector for both particles in figure 5.17.

However, the results for sample A3 (figure 5.16) are the most interesting due to the fact that no metallic Pd was found as in the other samples (figures 5.17). This suggests that the synthesis has succeeded in polymerizing without reducing the Pd to its metal state. However, the reaction using the MIP results in a mixture of products with a higher tendency towards meta and para positions shown in figure 5.18.

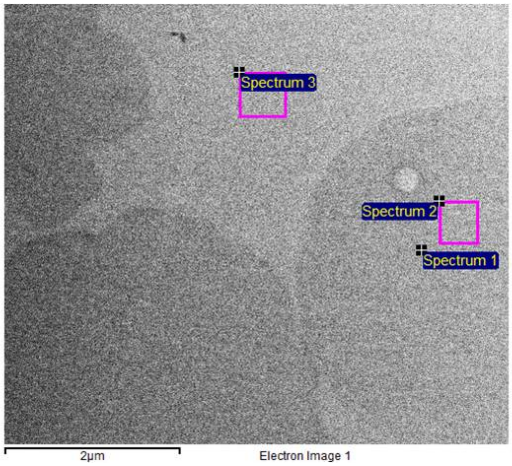

	C	O	Cl	Pd
Spectrum 1	95.53	4.05	0.12	0.30
Spectrum 2	95.62	3.91	0.14	0.33
Spectrum 3	96.24	3.74	0.00	0.02

Figure 5.16: XEDS-data for three sites on the image from sample A3. Spectrum 1 and 2 are from the MIP-particles while spectrum 3 is from the embedding polymer. The XEDS-data is given in atomic%.

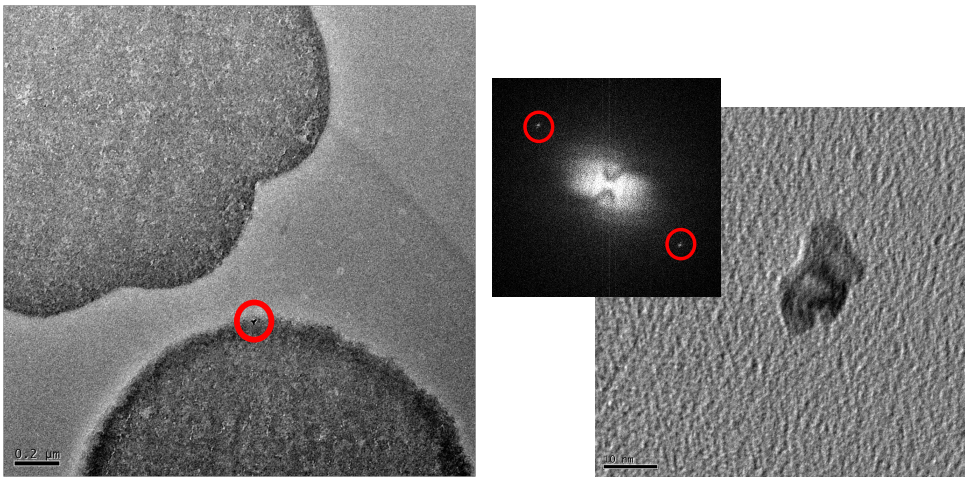

(a) A marked particle of higher contrast in sample C1. XEDS confirms a higher level of Pd (1.38 at%) in that particle but the rest follows the data in figure 5.16.

(b) FFT of one particle found in sample B3. Marked intensities are found at 4.45nm^{-1}, corresponding to Pd 111. XEDS shows a significantly higher level of Pd (2.05 at%).

Figure 5.17: Analysis of high contrast particles found in the MIP confirmed to be metallic Pd by XEDS and FFT.

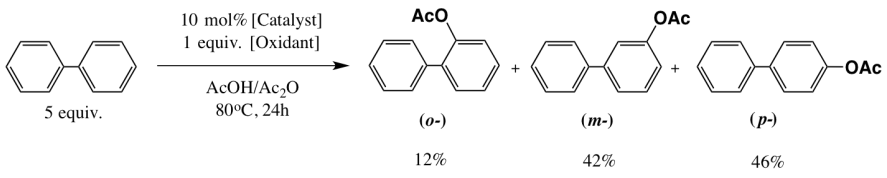

Figure 5.18: Acetoxylation of the biphenyl using the MIP. The result is a mixture of products. (Courtesy Maitham Majeed)

5.6 Tungsten on Zirconia in SEM

The W-ZrO_2 sample was coated with C and XEDS-analysis for C and W was performed, presented in table 5.4. The C-layer was not sufficient for acquiring good images and therefore additional samples were prepared of the same beads but instead coating them with Au-Pd (80:20). Images are shown in figure 5.19.

	W	C
Fresh	1.46	63.24
Sintered	0.28	62.83
Used	1.40	78.21

Table 5.4: The average atomic percent of W and C in the three samples for the data points taken at random (17 points in the fresh sample and 9 for the other two). Important to note is that these numbers are not absolute values because of the 30nm C-layer added on top of the surface. The relative differences is the info sought.

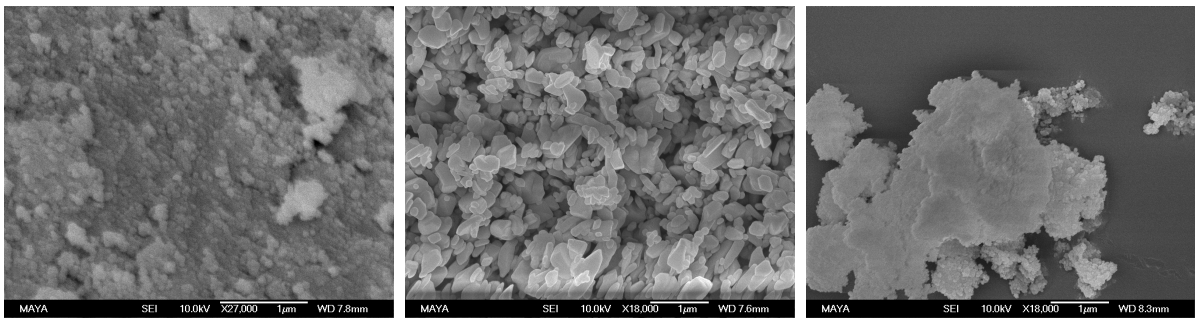

(a) Fresh sample. **(b)** Sintered sample. **(c)** Used sample.

Figure 5.19: The three different samples of $W - ZrO_2$ at similar (not the same) magnification. Small white scale-bar is $1\mu m$.

As seen in table 5.4, there are some variations between the samples. A certain amount of W is found in the fresh sample which is similar to the levels in the used sample. Both these levels are close to the specification of 10wt% WO_3, equaling 1.395at% W. However, in the sintered sample levels have dropped significantly. This quantification calculation was done in the software (AZtec by Oxford Instruments) using a preset C-layer in order to account for the absorption. The level of C was calculated in the software by removing the preset layer. The used sample was found to have higher quantities of C than the other two.

The particle size also differ, seen in figure 5.19 where the particle size of the fresh and used samples are around 50nm and the sintered sample has particles around 400nm. The particles in the sintered sample also appear smoother and irregular in shape, as if several particles have fused.

Chapter 6
Conclusions

For this project ten catalyst have been analyzed for their physical appearance and composition using the transmission electron microscope (TEM) and scanning electron microscope (SEM). The techniques used varied from pure image analysis to elemental mapping using characteristic x-rays in order to distinguish the catalytic particles from the supporting material.

The supported catalytic Au-particles have been measured in size using the TEM-images acquired using different imaging modes. Modes consisted of contrast analysis of CTEM and STEM-images to distinguish the Au-particles from the supporting oxide, as well as filtering for spatial frequencies or x-ray signals. The established sizes of the found particles, methods and catalytic performance (measured by other researchers) are shown in table 6.1. No agglomeration has been found.

Au on:	Size /nm	Method/images	Catalytic measurements
CeO_2 (Imp)	5-8	FFT and STEM	DPA: 66%
CeO_2 (SOL)	9-12	FFT	
ZrO_2 (DP)	8-16	FFT, STEM and XEDS-maps	A: 59%, B: 39%, C: 2%
Al_2O_3 (Imp)	7-10	FFT	DPA: 61%

Table 6.1: Size of the particles found in the different samples of supported Au-particles. Same as table 5.3 but here including the methods used for the measurements.

Not too much can be concluded the differences in sizes regarding the catalytic effect, since they are used in two different reactions and one of the catalyst have not been tested at all. However, the smaller Au on CeO_2 (Imp) do favor the DPA slightly more than the Au on Al_2O_3 (Imp). Both of the total conversions are similar, 18 and 19%. For the second reaction, of bromoanisole coupling with benzene, no comparison can be made at all. The work of testing the catalyst is still in progress. However, the content of this thesis is not focused on the catalytic reaction, but on the method of measuring the catalysts.

The MIP-samples show a low, but significant level of Pd that is originating from the MIP, shown by the lack of Pd quantified in the fixing polymer. From the section 4.1 on fabrication of the particles it is indicated that the atomic-percentage of Cl should be twice the percentage of Pd, something that is not supported by the data in figure 5.16. This is most likely due to the XEDS having problem correctly quantifying elements at such low concentration. The general conclusion of the A3 sample is that the Pd is in its oxidized form and bound to the polymer as intended which is also confirming

other analyses performed by other researchers. A promising result for future research.

The $W - ZrO_2$ sample showed the expected amount of W in the fresh and used samples and the lower amount in the sintered sample is best explained by evaporation of WO_3, which occurs at significantly lower temperatures than for pure W[30]. Sintering also resulted in the expected fusion of particles. The accumulation of carbon-based material in the pores, described in the article by Hulteberg et al. [27] is confirmed by the elevated C-content. All in all these samples had the expected characteristics and the results confirms other measurements performed by Hulteberg et al. From a microscopy point of view the only thing to remember is the choice of coating depending on the info sought.

Not all of the modes have been used on all the samples, as seen in table 6.1. The difference in the methods can be, as previously mentioned, used to confirm each other and to determine which particles are in fact Au and which are just thicker areas of oxide. This is not trivial to find out from just the CTEM-images, especially when the cations of the oxide do not differ too much from the metal (as in th case of cerium and gold). The STEM-images can provide more information revealing the nature of the particles, such as in figure 6.1 where the brighter round Au-particles are relatively easy to distinguish from the rougher ceria particles. This is an image of a Au on ceria sample used in catalysis where the Au-particles (also confirmed by XEDS) have grown larger than intended. However, lack of microscope availability did not permit the use of all the techniques on all the samples. The image analysis, especially the one in figure 5.13, concludes that STEM together with XEDS-mapping provided clear and interpretable results that would have been the best option for all the samples. It did not require any certain alignment of the Au-particles in order to find them, as were the case using FFT-filtering. The FFT-filtering however is good for acquiring more data since it only requires the CTEM images taken, which can then be analyzed later. This leaves more time for acquiring lots of images while at the microscope while XEDS-mapping is very time consuming in order to get good results.

6.1 The Future of Catalysts and TEM-Analysis

Catalysts are and will be of importance for making and controlling the production of a multitude of chemicals useful in a wide verity of industries and research. Without them, efficiency will decrease which is far from ideal for mankind in these times of high consumption and environmental impact. One additional application is energy harnessing from solar cells, namely storage of energy by splitting water into oxygen and hydrogen ($2H_2O \rightarrow 2H_2 + O_2$) which can be used later in so called fuel cells. An optimized catalyst will improve the efficiency, making solar energy a better energy alternative.[10] However, when developing new technologies there must always be consideration of side effects and in the case of nanoparticles there are some risks involved. Due to their activity and their size, some nanoparticles are considered somewhat harmful to the environment and animals, including us humans.[31] This means consideration of risks must be taken during development, although not obstruct completely since development is key to our progress. Future, much needed, studies on toxicity have to guide the researching community juggling both perspectives.

In the quest of optimization, analysis always plays a large role. TEM-techniques provides compelling

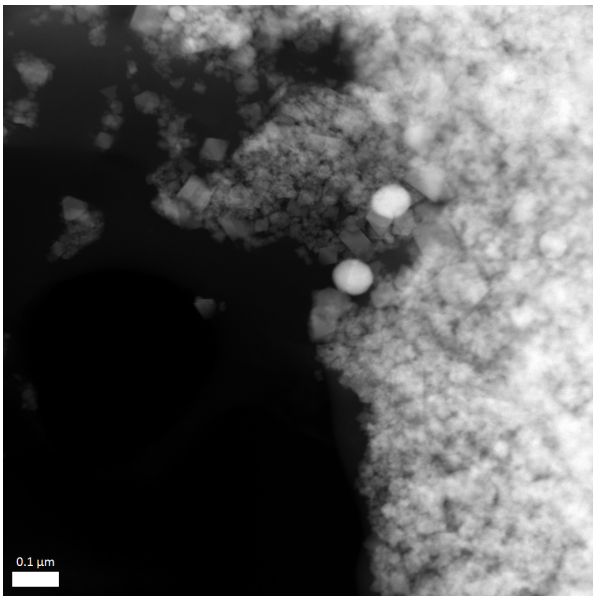

Figure 6.1: HAADF-STEM image of round Au-particles on ceria. Au is distinguished by higher intensity (scatters more), rounder shape and XEDS.

interpretable images of the catalysts as well as tells us more of local compositions or irregularities, using its focusing abilities. This convinces us that the TEM is a vital tool in future development of catalysts as well as future similar work. However, TEM will never provide large quantities of data. The area of sample covered is small and the technique will not provide large basis for statistics. Further detailed analysis of samples such as the ones in this thesis should preferably be performed using STEM in order to distinguish the particles. CTEM-images are useful for possible crystal analysis of the particles themselves but often the real challenge comes in finding them in the first place, something easier done using STEM. Statistics are then left for other instruments.

References

[1] D. B. Williams and C. B. Carter. *Transmission Electron Microscopy, A Textbook for Material Science*. Springer Science and Business Media, second edition, 2009.

[2] Lawrence Berkeley National Laboratory. X-ray Data Booklet, 2009, http://xdb.lbl.gov/xdb.pdf.

[3] G. Ertl. Reactions at Surfaces: From Atoms to Complexity. In *Nobel Lecture*, December 8, 2007.

[4] P. W. Atkins and L. L. Jones. *Elements of physical chemistry (4th Edition)*. W. H. Freeman, 2008.

[5] J. A. Moulijn, P. W. N. M. van Leeuwen and R. A. van Santen. *CATALYSIS, An Intergrated Approach to Homogeneous, Heterogeneous and Industrial Catalysis*, volume 79. Elsevier Science Publishers B.V., 1993.

[6] P. Herves, M. Perez-Lorenzo, L. M. Liz-Marzan, J. Dzubiella, Lu Y. and M. Ballauff. Catalysis by metallic nanoparticles in aqueous solution: model reactions. *Chem. Soc. Rev.*, 41:5577–5587, 2012.

[7] Z. Y. Zhou, N. Tian, J. T. Li, I. Broadwell and S. G. Sun. Nanomaterials of high surface energy with exceptional properties in catalysis and energy storage. *Chemical Society Reviews*, 40(7):4167–4185, 2011.

[8] S. Cheong, L. Graham, G. L. Brett, A. M. Henning, J. Watt, P. J. Miedziak, M. Song, Y. Takeda, S. H. Taylor and R. D. Tilley. Au-Pd Core–Shell Nanoparticles as Alcohol Oxidation Catalysts: Effect of Shape and Composition. *ChemSusChem*, 6(10):1858–1862, 2013.

[9] T. Akita, T. Hiroki, S. Tanaka, T. Kojima, M. Kohyama, A. Iwase and F. Hori. Analytical TEM observation of Au–Pd nanoparticles prepared by sonochemical method . *Catalysis Today*, 131(1–4):90 – 97, 2008.

[10] N. S. Lewis and D. G. Nocera. Powering the planet: Chemical challenges in solar energy utilization. *Proceedings of the National Academy of Sciences*, 103(43):15729–15735, 2006.

[11] G. Prieto, J. Zecevic, H. Friedrich, K. P. de Jong and P. E. de Jongh. Towards stable catalysts by controlling collective properties of supported metal nanoparticles. *NATURE MATERIALS*, VOL 12, 2013.

[12] M. Tanase, N. T. Nuhfer, D. E. Laughlin, T. J. Klemmer, C. Liu, N. Shukla, X. Wu and D. Weller. Crystallographic ordering studies of FePt nanoparticles by HREM. *Journal of Magnetism and Magnetic Materials*, 266(1–2):215 – 226, 2003.

[13] IUPAC. *Compendium of Chemical Terminology*. Blackwell Scientific Publications, Oxford, 2nd edition, 2014.

[14] I. Fechete, Y. Wang and J. C. Védrine. The past, present and future of heterogeneous catalysis . *Catalysis Today* , 189(1):2 – 27, 2012.

[15] A. Ostafin, J. Hoefelmeyer, K. Philippot, T. Pal, M. Knecht, Liu P., S. Suib, A. Roucoux, H. Yamashita, F. Alonso and others. *Metal Nanoparticles for Catalysis: Advances and Applications*. RSC Catalysis Series. Royal Society of Chemistry, 2014.

[16] A. M. Henning, J. Watt, P. J. Miedziak, S. Cheong, M. Santonastaso, M. Song, Y. Takeda, A. I. Kirkland, S. H. Taylor and R. D. Tilley. Gold-palladium core-shell nanocrystals with size and shape control optimized for catalytic performance. *Angewandte Chemie - International Edition*, 52(5):1477–1480, 2013.

[17] J. Li, J. Chen, W. Song, J. Liu and W. Shen. Influence of zirconia crystal phase on the catalytic performance of Au/ZrO2 catalysts for low-temperature water gas shift reaction. *Applied Catalysis A: General* , 334(1–2):321 – 329, 2008.

[18] J. Zheng, J. Li, H. Wei, J. Yu, H. Su and X. Wang. The investigation of gold/zirconia as a photocatalyst for the direct synthesis of imines from alcohols and aniline. *Materials Science in Semiconductor Processing*, 32(0):131 – 136, 2015.

[19] H. M. T. Galvis, J. H. Bitter, C. B. Khare, M. Ruitenbeek, A. I. Dugulan, K. P. de Jong. Supported Iron Nanoparticles as Catalysts for Sustainable Production of Lower Olefins. *Science*, 335:835–838, 2012.

[20] K. Sonogashira. Development of Pd–Cu catalyzed cross-coupling of terminal acetylenes with sp2-carbon halides . *Journal of Organometallic Chemistry*, 653(1–2):46 – 49, 2002.

[21] S. Frigoli, C. Fuganti, L. Malpezzi and S. Serra. A practical and efficient process for the preparation of tazarotene. *Organic process research & development*, 9(5):646–650, 2005.

[22] G. Wulff. Enzyme-like catalysis by molecularly imprinted polymers. *Chemical Reviews*, 102(1):1–28, 2002.

[23] T. Komatsu, K. Inaba, T. Uezono, A. Onda and T. Yashima. Nano-size particles of palladium intermetallic compounds as catalysts for oxidative acetoxylation. *Applied Catalysis A: General*, 251(2):315–326, 2003.

[24] A. L. Patterson. The Scherrer formula for X-ray particle size determination. *Physical review*, 56(10):978, 1939.

[25] D. Ozkaya. Final Analysis: Particle Size Analysis of Supported Platinum Catalysts by TEM. *Platinum Metals Review*, 52(1):61–62, 2008.

[26] L. Reimer and H. Kohl. *Transmission Electron Microscopy, Physics of Image Formation*. Springer Science and Business Media, fifth edition, 2008.

[27] C. Hulteberg, A. Leveau and J. G. M. Brandin. Pore condensation in glycerol dehydration. *Topics in catalysis*, 56(9-10):813–821, 2013.

[28] A. Shavel, B. Rodríguez-Gonzáles, M. Spasova, M. Farle and L. M. Liz-Marzán. Synthesis and Characterization of Iron/Iron Oxide Core/Shell Nanocubes. *Advanced Functional Materials*, 17(18):3870–3876, 2007.

[29] S. P. Limandri, A. C. Carreras and J. C. Trincavelli. Effects of the carbon coating and the surface oxide layer in electron probe microanalysis. *Microscopy and Microanalysis*, 16(5):583, 2010.

[30] A. Azens, M. Kitenbergs and U. Kanders. Evaporation of tungsten oxides: A mass-spectrometric study of the vapour contents. *Vacuum*, 46(7):745 – 747, 1995.

[31] G Bystrzejewska-Piotrowska, J Golimowski and P. L. Urban. Nanoparticles: Their potential toxicity, waste and environmental management. *Waste Management*, 29(9):2587 – 2595, 2009.